Received: 7 April 2025 | Revised: 23 June 2025 | Accepted: 25 June 2025

DOI: 10.1002/rpm2.70020

REVIEW ARTICLE

RESPONSIVE MATERIALS Open Access WILEY

Responsive cellulose nanocrystal-based liquid crystals: From structural color manipulation to applications

Jiao Liu[1,2] | Ye-Ming Qing[1] | Jun-Jie Wu[1] | Jing-Qi Tian[1] | Chi-Bo Feng[1] | Xin-Yu Zhou[1] | Yun Ma[1,3] | Bing-Xiang Li[1] | Yan-Qing Lu[2] | Quan Li[4]

[1]College of Electronic and Optical Engineering & College of Flexible Electronics (Future Technology), Nanjing University of Posts and Telecommunications, Nanjing, China

[2]National Laboratory of Solid State Microstructures & Collaborative Innovation Center of Advanced Microstructures & College of Engineering and Applied Sciences, Nanjing University, Nanjing, China

[3]State Key Laboratory for Organic Electronics and Information Displays & Jiangsu Key Laboratory for Biosensors, Institute of Advanced Materials (IAM), Nanjing University of Posts and Telecommunications, Nanjing, China

[4]Institute of Advanced Materials & School of Chemistry and Chemical Engineering, Southeast University, Nanjing, China

Correspondence

Yun Ma, Bing-Xiang Li, Yan-Qing Lu and Quan Li.
Email: iamyma@njupt.edu.cn, bxli@njupt.edu.cn, yqlu@nju.edu.cn and quanli3273@gmail.com

Abstract

Cellulose, one of the most versatile and abundant biopolymers in nature, has been employed by humans for thousands of years in diverse applications, such as renewable energy resources, structural materials, and fabric constituents. Cellulose nanocrystals (CNCs), obtained through the acidic hydrolysis of cellulose-based materials including wood, cotton, and additional sources, have attracted significant attention in areas, for example, energy storage, cosmetics, and medical devices. CNCs can spontaneously assemble into a cholesteric liquid crystal phase, which exhibits distinctive properties including biodegradability, high surface area, low cost, excellent mechanical strength, and surface functionality. Modifying the surfaces of CNCs or embedding CNCs with other materials enables novel cellulose-based composites for advanced technologies and applications. This review systematically outlines the preparation of cellulose-based liquid crystals (LCs), highlights the structural color regulation, photonic properties manipulation, and potential applications. Specifically, stimuli responsiveness, for example, temperature-responsiveness, humidity-responsiveness, pressure-responsiveness, tension-responsiveness, electricity-responsiveness, magnetic force-responsiveness and the optical properties of cellulose-based LCs (circularly polarized light modulation and circularly polarized phosphorescence properties) are demonstrated. Furthermore, the applications of cellulose-based LCs for gas detection, anticounterfeiting, multicolor separation, multifunctional E-skin, and advanced fabrics are also reviewed. Finally, this review concludes with the remaining challenges and perspectives for unleashing new possibilities in the development of high-performance multiple-responsive cellulose-based LCs.

Keywords

cellulose nanocrystal, cholesteric liquid crystal, stimuli responsive, structural color

1 | INTRODUCTION

The concept of chirality refers to the geometric property of an object that lacks mirror symmetry or inversion symmetry that cannot be superimposed onto its mirror image by any translation or rotation. The chirality is widespread in nature and serves as a fascinating characteristic and it has been extensively studied in fields like physics, chemistry, biology, and materials science.[1] Chirality exists at different length scales in nature, ranging from molecules to meso- or macro-

Jiao Liu, Ye-Ming Qing and Jun-Jie Wu contributed equally to this work.

scale supramolecular assemblies.[2] Molecular-level chirality can be found in different biological structures, including proteins, DNA, and polysaccharides, where the chirality plays a crucial role in determining their distinctive properties.[3] Cellulose, the most abundant biopolymer in nature,[4] derived from wood, algae and tunicates, and other biomass,[4b,5] is regarded as a renewable resource as well as a remarkable substance with different uses as materials.[6] It has the ability to form a stable cholesteric liquid crystal (CLC) phase and preserve its ordered molecular structure in solid films.[5a,7] Its unique molecular structure confers a variety of excellent properties, such as strong hydrophilicity,[8] high mechanical strength, rigidity and modulus along the axial direction of molecular chain,[9] and remarkable structural stability.[10] Nanocellulose, which is obtained from natural cellulose fibrils, is characterized by having at least one dimension ranging from 1 to 100 nm. It has opened up new opportunities in the fabrication of photonic components, including chiral reflectors,[11] photonic electrodes,[12] antireflection coatings for solar cells,[13] multifunctional thermal[14] or humidity responsive optical materials,[15] flexible substrates for plasmonic sensing,[16] and surface-enhanced Raman scattering spectroscopy.[17] Nanomaterials are primarily categorized into cellulose nanocrystals (CNCs), cellulose nanofibrils (CNFs), and bacterial nanocellulose.[18]

CNCs are one-dimensional, rod-like nanomaterials with a high aspect ratio, sourced from renewable and biodegradable natural-occurred cellulose.[19] CNCs have garnered significant interest in areas such as sensing,[20] tissue engineering,[21] reinforced plastics,[22] and optics[23] due to their sustainability, biocompatibility, nanoscale size, large surface-to-volume ratio, ease of surface chemistry modification, and unique optical properties.[5k,24] CNC suspensions can form thin films,[25] foam,[26] and hydrogels,[27] exhibiting distinct mechanical, optical, and chemical properties compared to original bulk cellulose fibers.[4a] As an abundant liquid crystal (LC) biopolymer with inherent chirality, CNCs can spontaneously arrange into cholesteric structures by controlled evaporation of water from CNC suspensions.[7b,28] The cholesteric liquid crystallinity of CNC/water suspension was first reported by Revol et al.[29] The self-assembled CNCs, acting as one-dimensional photonic crystal,[23a,30] maintain their helicoidal ordering in the solid state.[4b,11a,28d,30a,31] The thin films exhibit iridescence and selectively reflect left-handed circularly polarized (LCP) light when the pitch of the cholesteric CNCs matches the visible light wavelength range.[11b,32] It is well established that aqueous hydroxypropyl can form a CLC at ambient conditions when the water content decreases to approximately 45 wt%,[33] which was first reported by Werbowyj and Gray.[34] The chemical structures of CNC and hydroxypropyl cellulose (HPC) are illustrated in Figure 1. Many organisms in nature are capable of generating vibrant structural color, which they utilize to deter predators and attract mates for survival and reproduction.[35] The color observed in iridescent beetles, butterflies, some sea creatures, and various birds result from light interacting with the structural patterns on their exoskeletons.[36] Circularly polarized

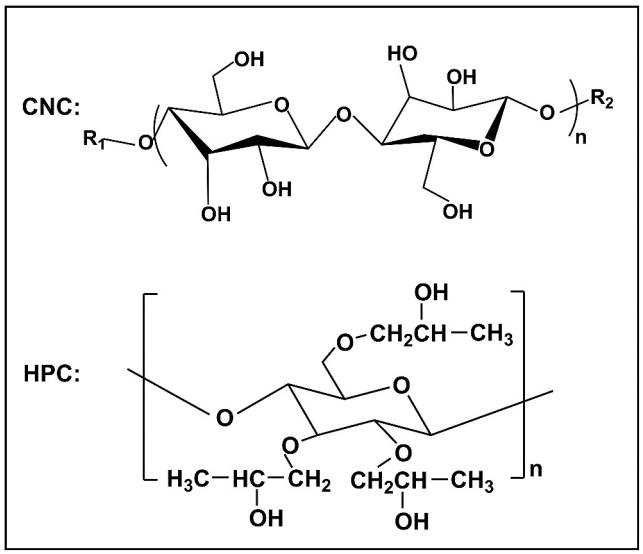

FIGURE 1 Chemical structures of CNC and HPC. CNC, cellulose nanocrystal; HPC, hydroxypropyl cellulose.

reflection has been observed in various animal species. Although it is visually fascinating, the function or purpose of this signal remains unclear, as no visual system has been found that can detect circularly polarized light.[37] Circularly polarized luminescence (CPL) materials have attracted significant attention in the fields of anticounterfeiting, bioimaging, organic light-emitting diodes, etc.[38] CPL is a luminescent phenomenon that shows the difference in the emission of right- and LCP light, linked to the excited state of chiral systems.[39]

In recent years, many reviews have discussed different aspects of the production,[10,40] structural properties,[9] applications,[10,40,41] and performance manipulation[4d] of cellulose-based particles or composites. The worldwide demand for eco-friendly technologies to minimize carbon footprint, enhance environmental sustainability, and mitigate the effects of climate change has driven this trend. Additionally, nanocellulose stands out as the most abundant and undoubtedly the most cost-effective organic nanomaterial. Cellulose-based nanocomposites have been extensively studied for applications in sensors, tissue engineering, biomedical fields, energy applications, and beyond. To our best knowledge, no review has yet comprehensively embraced the flourishing topic of the multiple-responsive behaviors of cellulose-based LCs. Therefore, it is essential to provide an easy-to-access overview of structural color regulation, performance manipulation and applications of cellulose-based LCs, as these are key to advancing their development and fostering further innovation. In this review, we provide a state-of-the-art account on the recent advancements of the cellulose-based LCs including preparation, structural color manipulation, stimuli responsiveness including temperature-responsiveness, humidity-responsiveness, pressure-responsiveness, tension-responsiveness, electricity-responsiveness, magnetic force-responsiveness and optical properties containing circularly

polarized light modulation and circularly polarized phosphorescence (CPP) properties (Figure 2). Subsequently, we discuss the practical applications of these multiple-responsive cellulose-based LCs in gas detection, anticounterfeiting, multicolor separation, multifunctional E-skin, and advanced fabrics, which have significant potential for further development of next-generation advanced functional materials in encryption display technologies. Finally, this review concludes with an outlook on the applications, current challenges, and future opportunities for high-performance cellulose-based LCs endowed with remarkable photophysical properties. Significantly, the main challenges regarding current methods and processes of cellulose-based LCs were highlighted, and the potential solutions to these issues are proposed in combination with cutting-edge research findings. It is expected that this review will contribute to the development and advancement of cellulose-based LCs.

2 | BACKGROUND

2.1 | Structural color

In nature, colors are categorized into two groups: pigment color and structural color. Pigment color, or chemical color, occurs when a surface absorbs light of particular wavelengths and reflects others, or when light passes through the transparent or translucent materials within certain wavelength ranges. Structural color, also known as physical color, primarily results from the scattering, refraction, and diffraction of incident light on the skin or surface, which is manipulated by thin films, multilayered structures, or ordered geometric photonic crystal structures.[42] Structural color has gained significant attention because of its iridescent, long-lasting, environmentally friendly, and customizable features, which provides significant advantages over conventional dyes and pigments.[43] This phenomenon has evolved over 500 million years, driven by natural selection to produce structural color that serves different biological purposes, like signaling, camouflage, attracting pollinators, or avoiding predators.[44] Numerous living creatures have developed the capability to change color and dynamically camouflage themselves, allowing them to visually merge with their surroundings for defense, communication, and evading predators.[45] Plants such as the Venus flytrap function as predators by swiftly snapping their traps shut when capturing insects.[46] In contrast, plants like *Mimosa pudica* act as prey by rapidly folding their leaves in response to threats to protect themselves from predators.[47] In more sophisticated systems, creatures like chameleons are capable of not just escaping threats but also altering their color for attraction, warning, and camouflage.[48] This involves the intricate internal regulation of organisms, such as osmotic pressure and alterations in cellular structures, resulting in the shape and color changes in response to stimuli, which provides valuable insights for the fabrication of smart actuators.[49] Insect cuticles, crab shells, bird feathers, and plants display a variety of natural patterns that feature striking structural color.[50] Periodic multilayer microstructures often produce vibrant iridescence,[50a,51] enabling the selective interference of light within the visible range, which leads to structural color that varies with the viewing angles.

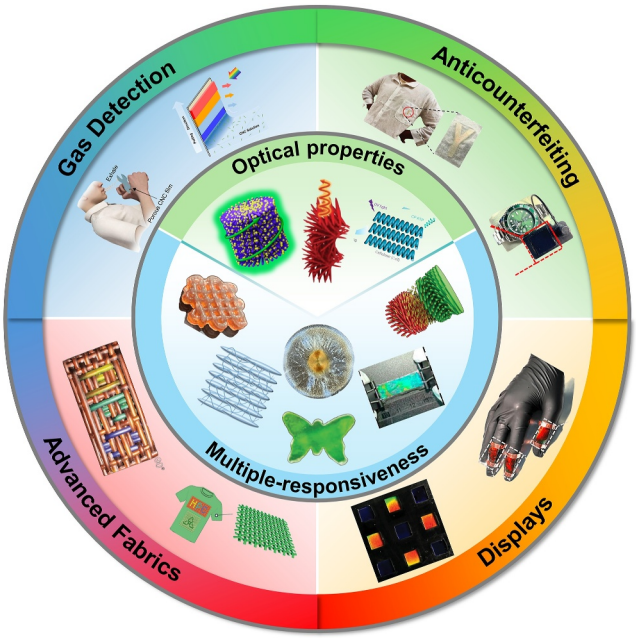

FIGURE 2 Schematic illustration of the multiple-responsiveness, optical properties, and applications of cellulose-based liquid crystals.

According to Bragg's law, circularly polarized light is selectively reflected, and a specific color's reflectivity can be obtained when the half-pitch distance matches the wavelength of that color. Cholesteric structures are present in various natural systems,[52] including those found in fruits, beetles, and the exoskeletons of crustaceans, which produce vivid structural colors because their pitch length matches the wavelengths of the visible light (Figure 3).[7b,36a,44a,53] Moreover, these structures demonstrate remarkable toughness and strength due to multiple toughening mechanisms at different scales, which are often absent in synthetic materials.[51] Due to their left-handed chiral arrangement, most natural chiral structures generally reflect left circularly polarized light. Figure 3 shows the metallic green beetle *Chrysina gloriosa* reflecting left circularly polarized light when exposed to unpolarized light,[36a] with the remarkable metallic color fading under a right circular polarizer. The beetle's exoskeleton features hexagonal sections that are green with a vibrant yellow core, where cholesteric nanostructures are arranged in a nearly hexagonal pattern, enabling left-handed reflection.[54] In recent years, scientists have focused on incorporating responsive materials into structural color films to develop novel structural color materials. This approach not only broadens the functional diversity of composite films but also allows color change to be easily observed by the naked eyes. Based on this principle, structural color materials have been developed to respond to

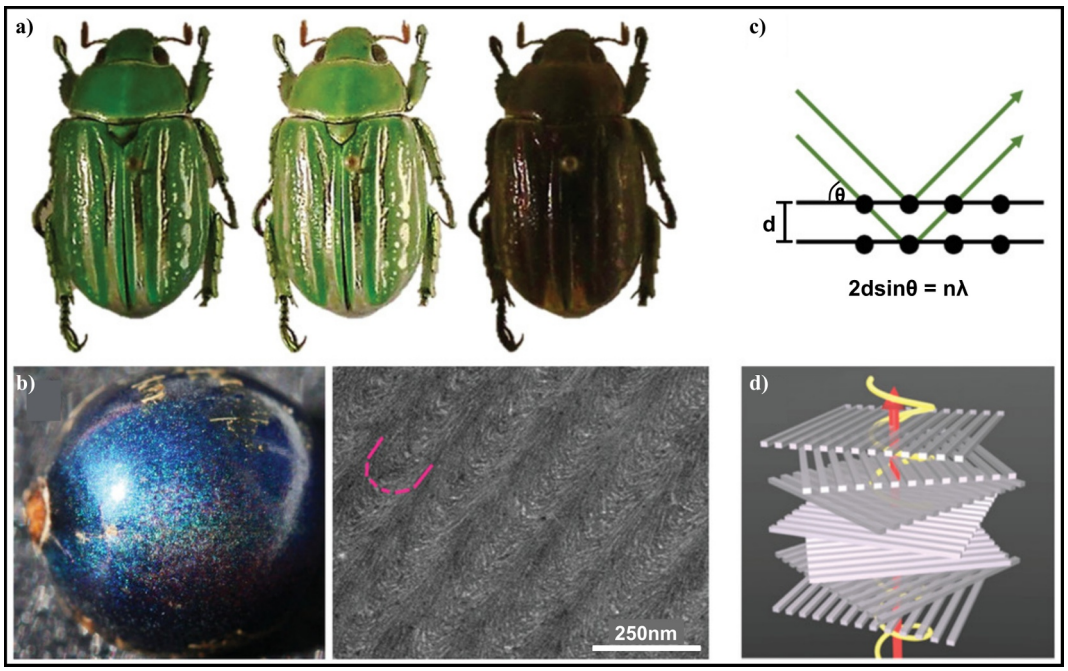

FIGURE 3 Examples of structural color in nature. (a) Photographs of scarab beetle under a L-CPF, no polarizer, and a R-CPF. Reproduced with permission.[36a] Copyright 2020, John Wiley and Sons. (b) Photograph of *Pollia condensata* fruit (left). TEM image (right) of cellulose microfibrils in *P. condensata*. Reproduced with permission.[25] Copyright 2012, National Academy of Sciences. (c) Bragg reflection for structural coloration. (d) A 3D illustration of the cellulose microfibril arrangement that generates structural color in *P. condensate*. Reproduced with permission.[7b] Copyright 2012, National Academy of Sciences. L-CPF, left-handed circularly polarized filter; R-CPF, right-handed circular polarized filter; TEM, transmission electron microscopy.

humidity,[55] temperature,[56] pH,[57] electricity,[58] magnetism,[59] and more. Structural color materials are applicable not only in various responsive optical devices but also in areas such as structural color encryption, anti-counterfeiting, and the production of textiles with LC structural color.

3 | CELLULOSE LCs

3.1 | Preparation of CNCs

CNCs can be obtained from cellulose fiber sources, such as cotton,[60] Whatman paper,[61] hardwood, softwood, and microcrystalline cellulose.[62] These materials have been widely researched for CNCs production through techniques like acid hydrolysis, enzymatic, oxidative degradation, and ionic liquid processing[63] (Figure 4a). In the typical CNCs extraction process, the amorphous regions of cellulose chains are removed by breaking their 1, 4-β-glycosidic bonds via acid hydrolysis. At the end of the process, only the crystalline portions of cellulose maintain in suspension. The morphology (shape and size), surface functional groups, and yield of CNCs depend on the cellulose source, acid types, treatment temperature, and reaction time.[64] The resulting CNCs display a needle-like structure, with lengths ranging from 100 to 500 nm and diameters between 5 and 50 nm (Figure 4b). Advancements in science and technology have motivated the development of new methods for synthesizing CNCs. However, acid hydrolysis remains the most traditional and commonly employed technique in the CNCs production.[65]

The typical production of CNCs typically depends on strong acid hydrolysis, which requires precise control over acid concentration and type, temperature, acid-to-cellulose ratio, and reaction time. These strong acids, including sulfuric acid (H_2SO_4), hydrochloric acid (HCl), hydrobromic acid (HBr), and phosphoric acid (H_3PO_4), as well as their combinations, have been widely used for CNCs extraction.[66] Among these, the H_2SO_4 is particularly favorable for the CNCs synthesis due to the electrostatic stabilization from the negatively charged sulfate half-ester groups on the CNC surface.[4a,67] During acid hydrolysis, the amorphous regions of cellulose fibrils are specifically broken down until the leveling-off degree of polymerization (LODP) is attained. Once the LODP stage is reached, the reaction almost stops, and the remaining intact CNCs are separated from the suspension.[68] The CNCs produced through H_2SO_4 hydrolysis introduces anionic sulfate (SO_4^{2-}) groups onto its surface via the esterification of hydroxyl groups by sulfate ions. The SO_4^{2-} groups on its surface enhance the colloidal stability of CNCs. However, a significant drawback of sulfuric acid-derived CNCs lies in its lower thermal stability. These sulfate groups can be eliminated through post-treatment with HCl hydrolysis, followed by water dialysis.[61,69] The CNCs extracted using HCl exhibits the

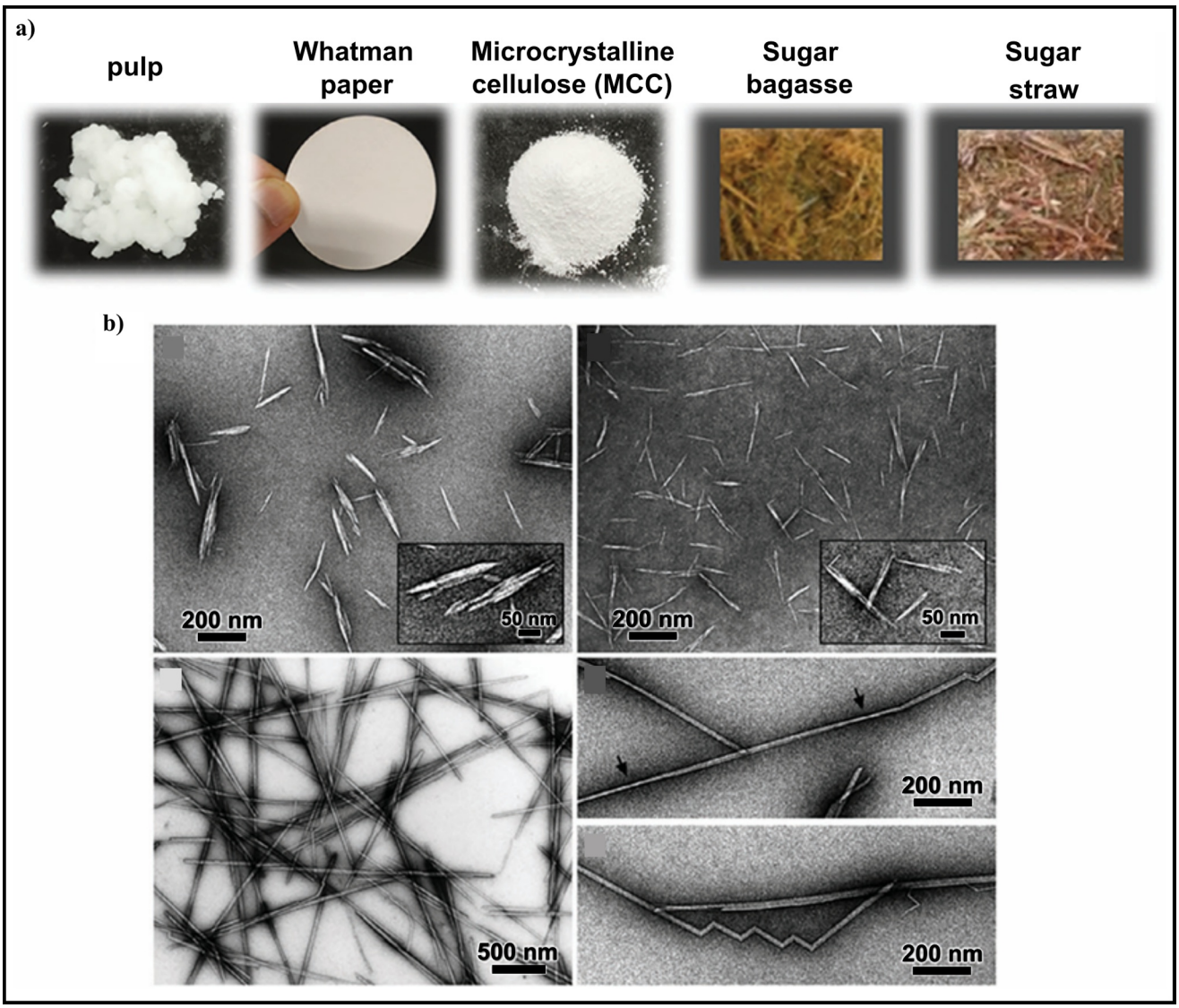

FIGURE 4 (a) Images of pulp, Whatman paper, Avicel MCC, sugar bagasse, and sugar straw used for the CNC extraction. (b) TEM images of negatively stained cellulose whiskers derived from cotton, MCC, and tunicate cellulose through sulfuric acid hydrolysis. Reproduced with permission.[5m] Copyright 2008, American Chemical Society. CNC, cellulose nanocrystal; MCC, microcrystalline cellucose; TEM, transmission electron microscopy.

enhanced thermal stability but suffers from lower yield and reduced surface charges, which may cause aggregation in suspension. To improve the efficiency of HCl or other acid hydrolysis, inorganic chloride catalysts are used in combination with HCl.[70] The addition of inorganic chlorides serves as a catalyst, accelerating the hydrolysis process and breaking down the amorphous regions more rapidly compared to conventional HCl hydrolysis. Currently, the preparation methods of CNCs typically involves the choice of acid for hydrolysis, such as (i) combinations of sulfuric, phosphoric, and hydrochloric acids,[71] (ii) deep eutectic solvents,[72] or (iii) an $FeCl_3$-catalyzed deep eutectic solvent system.[73]

3.2 | LC phase of CNCs

LCs are well-known functional soft materials that exhibit both the fluidity of liquids and the ordered structure of crystals, which span molecular, supramolecular, and macroscopic scales.[74] This phase, first termed by Lehmann in 1888,[75] is now widely recognized as the fourth state of matter, alongside gas, liquid, and solid. LCs science has developed over the past century from the study of a simple phenomenon to an interdisciplinary field integrating biology, physics, chemistry, engineering, and nanotechnology. A deeper understanding of LC components and their assembly is essential for advancing the field of LC materials and their

future applications. LC phases like nematic, smectic, and cholesteric describe the organization of LC components, which can be rods, discs, plates, and more. LCs are generally categorized into thermotropic and lyotropic types.[76] Thermotropic LCs are utilized in displays because they maintain their LC state over a certain temperature range. Lyotropic LCs, such as tobacco mosaic virus suspensions, transition to the LC phase when their concentration in the solvent exceeds a critical threshold. According to Onsager model, the aspect ratio of colloidal particles significantly influences the onset of LC and the volume fraction of different phases. The Onsager model indicates that the rod-like structure of CNCs exhibits lyotropic LC behaviors.[4b] When the concentration of CNCs exceeds a certain threshold, it forms both isotropic and anisotropic phase, with the anisotropic phase adopting a cholesteric structure.[77] In the cholesteric phase, the helical structure of CNCs shows the characteristic of angle-dependent selective reflection of circularly polarized light, producing iridescence when the helical pitch matches the wavelength of visible light. In water, the CNC suspension forms a cholesteric phase that can be maintained after air-drying, resulting in an iridescent film (Figure 5).[3] These features, combined with large surface area of CNCs, make them an ideal candidate for templating porous inorganic materials. Researchers constructed silica/CNC hybrid materials by combining the suspension of CNCs with a mesoporous silica precursor, tetramethoxysilane. Polarized optical microscopy (POM) images show the formation of fingerprint textures during evaporation, indicating the emergence of cholesteric phase in the presence of the silica precursor (Figure 5b–d). Once dried, the CNCs composite films that stood freely can be constructed. Visually, both POM and scanning electron microscopy images illustrate that these films closely resemble those made from pure CNCs.

4 | STIMULI-RESPONSIVE CELLULOSE-BASED LCs

Stimuli-responsive functional materials have gained significant attention because of their fundamental scientific importance and promising technological applications, as their physical properties can be actively regulated by different stimuli.[78] It is well-established that CLCs, featuring self-organized helical superstructures,[78a,79] are capable of responding to external stimuli such as temperature, light, electric fields, and others.[80] The properties of cholesteric CNC films can be modified by altering the CNC surfaces. However, external factors like temperature, humidity, pressure, tension, electricity, magnetism, and light have a significant impact on the characteristics of CNC films. The CNC films with tunable helical pitch can be realized by applying heat[81] or sonication,[82] enabling the adjustable chiral photonic properties of CNCs. Owing to the diamagnetic anisotropy of CNC rods, both magnetic[83] and electric field[84] can be utilized to orient the CNC rods within

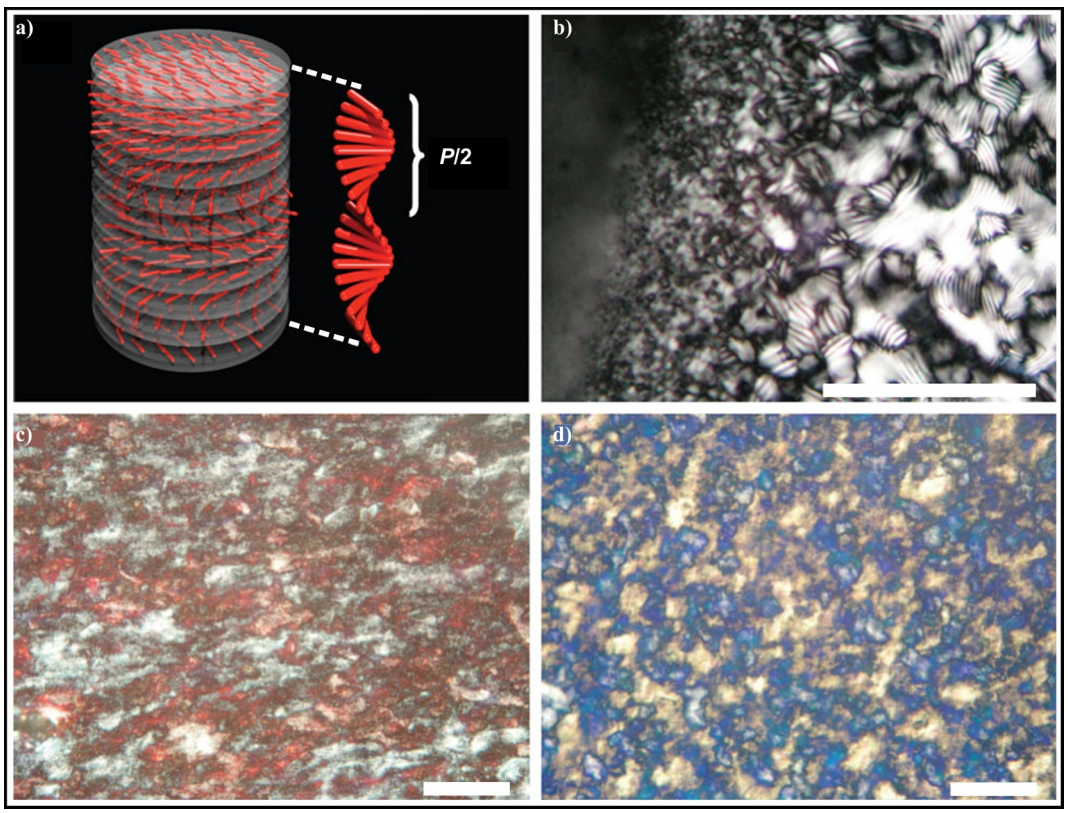

FIGURE 5 Schematic of the cholesteric ordering of CNCs (a) and POM images (b–d). Reproduced with permission.[3] Copyright 2010, Springer Nature. CNCs, cellulose nanocrystals; POM, polarized optical microscopy.

a suspension. When a constant field is applied to a drying CNC suspension, it causes the CNC rods to align perpendicular to the field, and this helical orientation can be maintained in solid films. The CNC-based composites that response to stimuli and their optical properties will be discussed in detail in the following section.

4.1 | Temperature-responsive cellulose-based LCs

Developing encryption and decryption technologies that are both secure and user-friendly are urgently needed to address the increasing threat of information leaks, despite the significant challenges exist. HPC, a water-soluble cellulose derivative, can be produced by incorporating hydroxypropyl groups into the cellulose polymer chains through etherification.[17] HPC can form a cholesteric structure in solutions with <45 wt% water content, which remain preserved when the solution is formed into a film.[33] HPC and CNCs differ notably in that HPC develops a right-handed cholesteric arrangement, reflecting right-handed circularly polarized (RCP) light, while CNCs arrange into a left-handed configuration, reflecting LCP light. Li et al.[85] introduced a method for the encoding and decoding information that leverages time and temperature in conjunction with functional photonic ink (Figure 6a). The ink's structural colors are composed of HPC/propylene glycol mesophases that can vary from colorless and transparent to encompassing the entire visible-light spectrum by adjusting the ink's composition and temperature. Furthermore, the ink is adaptable for creating intricate designs, quick-response (QR) codes, and multi-pixel arrays. This ink facilitates the precise encoding of encrypted data by manipulating specific temperature and time duration. The use of sophisticated encryption techniques, including multichannel and Morse coding, enhances information storage security and increases decoding complexity. This study paves the novel way for innovative dynamic photonic inks and encryption strategies for anticounterfeiting applications.

Structural color results from the interaction of light with periodic submicrometer structure within materials, providing a unique mechanism for coloration.[44b,86] In the natural word, many organisms employ intricate regulatory systems to alter their colors in response to external stimuli.[48,87] Drawing inspiration from this phenomenon, artificial materials with structural color have been developed by replicating biomimetic photonic structures using methods such as

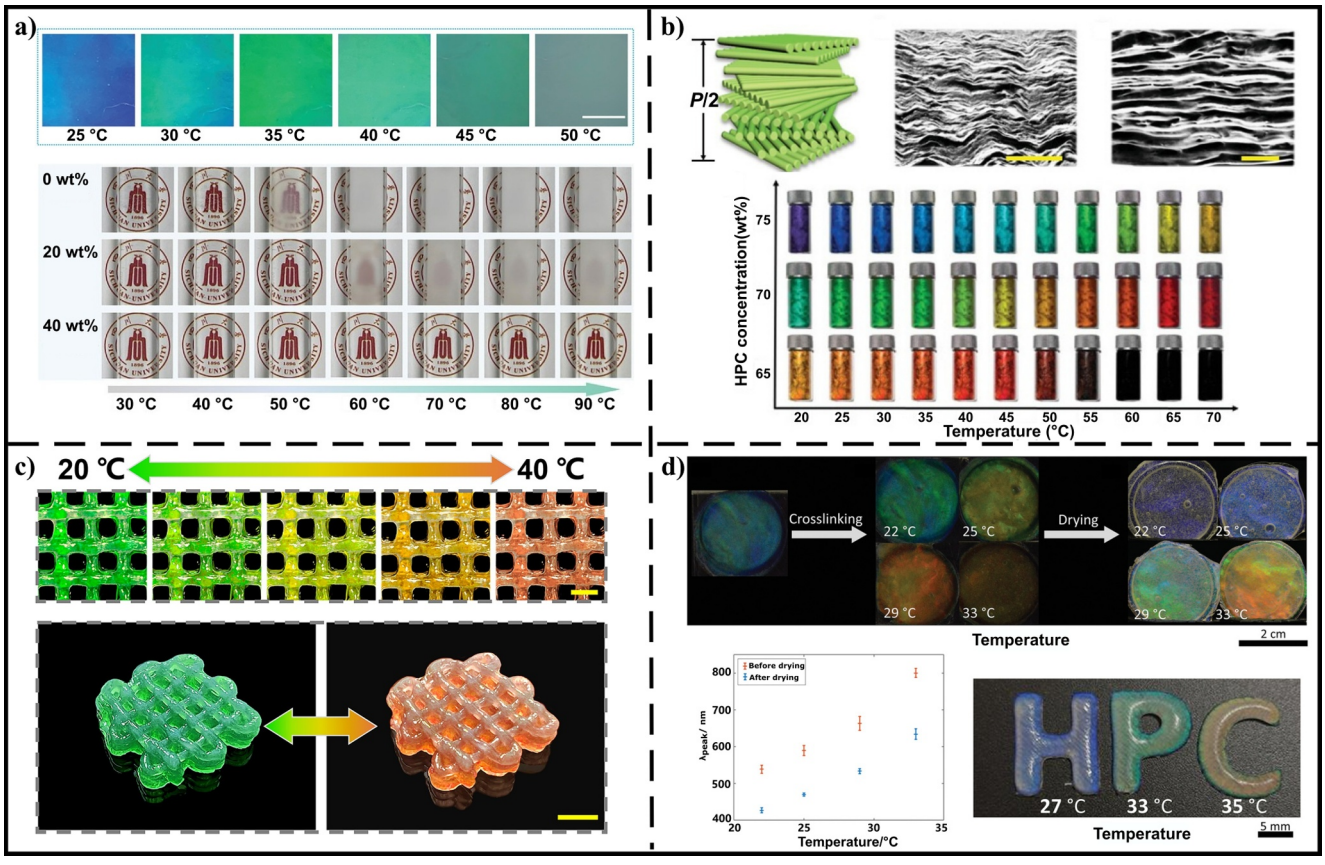

FIGURE 6 (a) Phase transition behaviors of HPC/PG solutions. Reproduced with permission.[85] Copyright 2022, John Wiley and Sons. (b) Optical properties and nanostructure of HPC-AM CLCs. Reproduced with permission.[91] Copyright 2021, John Wiley and Sons. (c) Thermal responsiveness of 3D printed objects. Reproduced with permission.[92] (d) Photographs depicting a 70wt% HPC-MA solution under different conditions, as well as photographs of 3D-printed letters. Reproduced with permission.[93] Copyright 2022, John Wiley and Sons. CLCs, cholesteric liquid crystals; HPC-AM, hydroxypropyl cellulose-acrylamide; HPC-MA, methacrylate-functionalized hydroxypropyl cellulose; HPC/PG, hydroxypropyl cellulose/propylene glycol.

lithographic patterning, colloidal assembly, and layer-by-layer stacking, etc.[50a,88] Among these materials, the assembled CLCs exhibit periodic structures composed of twisted layers, where the rod-like molecules are aligned in parallel.[3,89] CLCs possess the unique capability to selectively reflect circular polarized light and manipulate this reflection through adjusting their helical pitch. This distinctive characteristic opens new possibilities in the realms of biology, physics, and various applied sciences.[78a,80b,90] Zhang et al.[91] developed novel cellulose-based CLCs, which can serve as a biomimetic model for biological structural coloration (Figure 6b). By using monomers rather than polymers within the cellulose CLC system, the hydrogen bonding interactions between cellulose molecules and acrylamide (AM) monomers are strengthened, enabling the self-assembly of the CLC and the generation of a wide range of vivid structural colors. By modulating the irradiation time during the polymerization of the mixtures with different crosslinking degrees, the periodic internal structures of cellulose-based CLCs can be carefully controlled, allowing for the fabrication of polymers with tunable structural colors. When HPC-AM is heated from room temperature to 70°C, the color transitions to red due to the increase in the helical pitch, which is caused by the disruption of hydrogen bonds and the intermolecular repulsion. These photonic-responsive materials, which display dynamic and high-resolution structural color, show great potential for applications in graphic displays, wearable sensors, and information encryption technologies. In 3D printing, achieving precise color reproduction is essential for producing vibrant visuals with high accuracy and long-lasting durability. The ink maintains a CLC state with structural color, while the addition of gelatin improves its rheological properties, enabling the smooth flow and the formation of self-supporting structures (Figure 6c).[92] The addition of hydrogel contributes to maintaining the integrity of the ink after printing, achieved through in situ UV crosslinking. Consequently, diverse graphics and 3D objects with angle-independent colors are produced, showcasing the versatility of the ink on different substrates. Furthermore, the produced objects display dual thermal responsiveness, leading to observable color changes at temperatures close to that of the human body. These attributes suggest that the current ink represents significant progress in the development of cutting-edge 3D printing technology. Chan et al.[93] showed that integrating methacrylate-functionalized hydroxypropyl cellulose (HPC-MA) with UV crosslinking facilitated the development of filaments with internal helical nanostructures, allowing for the 3D printing of solid objects with structural color (Figure 6d). The iridescent color can be tuned across the entire visible wavelength spectrum by taking advantage of the lyotropic and thermotropic characteristics of HPC during the crosslinking process, producing a variety of colored objects from a single material source. This approach improves precision in controlling both micro- and macro-scale structures and opens opportunities for developing sustainable photonic filaments for 3D printing.

4.2 | Humidity-responsive cellulose-based LCs

Photonic films that can adapt to external stimuli are widely used in optical communication, sensing, and anti-counterfeiting applications. However, developing photonic structures with customizable patterns that display significant color changes under ambient environmental conditions remains a challenge. Lu et al.[94] introduced a supramolecular lyotropic LC system using cellulosic macromolecules, where the addition of citric acid (CA) enhances the long-range order of helical structures during evaporation-induced self-assembly (EISA) and allows the precise tuning of their helical pitch by changing its concentration. The hydrogen bonding interactions between CA's carboxylic acid groups and the hydroxyl groups facilitate the formation of a moisture-responsive supramolecular helical structure (Figure 7a,b). When the relative humidity (RH) increases, water molecules are absorbed into the polymer networks, disrupting hydrogen bonds and leading to an increase of the helical pitch. In addition, a reduction in RH causes the film to dehydrate, enabling hydrogen bonds to reform and the pitch to contract. The helical pitch in HPC-CA films expands and contracts in response to humidity variations, resulting in reversible color shift. By optimizing the helical pitch, the HPC-CA films can be tailored to produce desired color changes. As depicted in Figure 7b, the HPC-15% CA film initially appears violet and changes smoothly from violet to red upon hydration. When dehydrated, the film gradually reverts to its original color. This remarkable colorimetric behavior emphasizes the adaptability and responsiveness of the hydrogen-bonded supramolecular lyotropic LC system, showcasing its potential for use in reflective displays, smart windows, sensors, and adaptive optical devices. Moreover, the dynamic hydrogen bonding within the supramolecular networks imparts desirable qualities to the HPC films, such as recyclability and reprocessability, which can be conveniently achieved by dissolving them in water. This study presents a scalable approach for the development of environmentally adaptive CLC polymers with tunable broadband colorations and highly customizable photonic patterns.

Zhao et al.[95] developed a technique for the self-assembly of chiral, humidity-sensitive coatings through electrostatic interactions between CNCs and polyacrylic acid (PAA) (Figure 7c,d). The chiral structures are formed due to the electrostatic repulsion between CNC and PAA, while their mutual affinity facilitates a swift response. The transmitted colors change in response to variations in RH and rotation angles, making them ideal for constructing ternary anticounterfeiting systems that can encrypt information and detect humidity. The CNC/PAA iridescent coating displays adjustable visible colors that change dynamically with variations in RH. The colors transition sequentially from violet at 22% RH, to cyan at 43% RH, orange at 75% RH, and ultimately red at 99% RH. The effect is reversible, maintaining a color memory ratio >97% after 10 cycles. The maximum wavelength (λ_{max}) of the

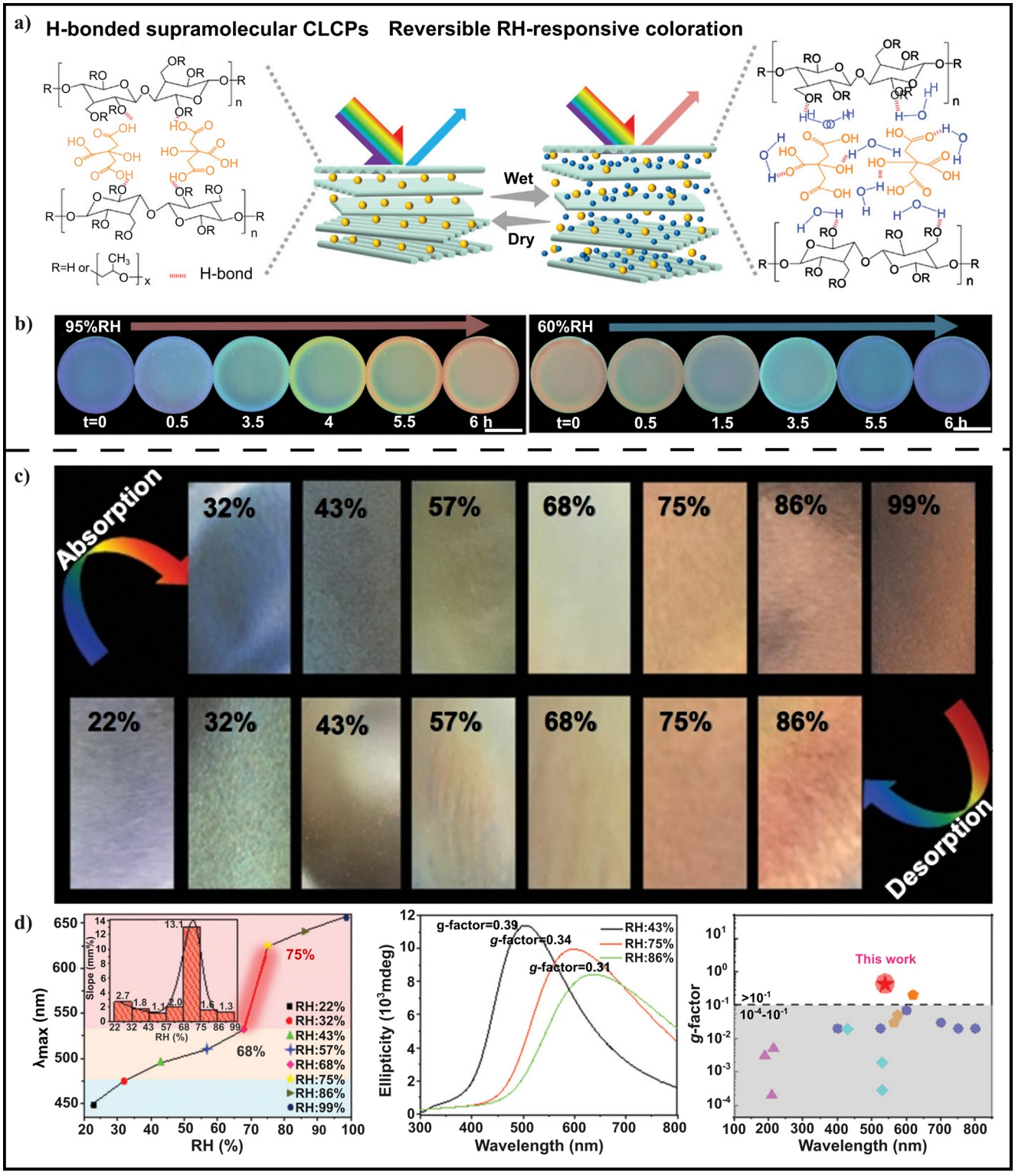

FIGURE 7 (a) Schematic diagram of the moisture-regulated helical pitch in H-bonded supramolecular HPC-CA CLCPs. (b) Photographs of the HPC-15% CA film showing a reversible color shift from violet to red at 95% RH, and a reverse at 60% RH. Reproduced with permission.[94] Copyright 2024, John Wiley and Sons. (c) Humidity response of CNC/polyacrylic acid iridescent coatings. (d) λ_{max} of the iridescent coating at given RH, CD spectra, and *g*-factor. Reproduced with permission.[95] Copyright 2021, John Wiley and Sons. CA, citric acid; CD, circular dichroism; CLCPs, cholesteric liquid crystal polymers; CNC, cellulose nanocrystal; HPC-CA, hydroxypropyl cellulose-citric acid; RH, relative humidity.

CNC/PAA iridescent coating gradually increases as RH increases from 22% to 68%. Significantly, a sharp increase in λ_{max} is observed when RH shifts from 68% to 75%. However, the increase in λ_{max} becomes less noticeable as RH approaches 99%. As a result, the CNC/PAA iridescent films display minor color transitions from violet to green within the 22% and 68% RH range. Above 75% RH, the color change becomes significantly more pronounced, shifting from orange to red. This charge-driven assembly unlocks new opportunities for cholesteric materials, enabling accurate optical sensing and sophisticated information encryption.

4.3 | Pressure-responsive cellulose-based LCs

In nature, some organisms possess dynamic structural colors that play significant roles in communication, defense, or camouflage.[45,88b,96] For instance, neon tetra and freshwater fish can flexibly alter their body color across a wide spectrum range in response to changes in light, temperature, and pressure.[97] These vivid and adaptable structural colors result from the interaction of light with adjustable nanostructures within their skin cells. Inspired by these biological systems, the development of biomimetic structural color devices with tunable schemochrome has garnered significant interest from both academic and industrial fields.[98] The self-organization of CNC promotes a helical multilayered structure, which exhibits long-range cholesteric order that is similar to the regularly arranged reflective layers observed in the skin cells of neon tetras.[99] The majority of CNC-based responsive materials have been developed through surface coating technique,[100] primarily relying on the increase of helical pitch due to water absorption or thermal swelling. Many approaches have been developed to produce CNC-based intelligent composites capable of displaying dynamic structural color in respond to stimuli like strain,[35,101] temperature,[102] humidity,[103] or gas.[104] Cao et al.[105] developed a pressure-responsive CNC airgel by combing LC self-assembly with ice-templating methods. Similarly, Shi et al.[106] fabricated structurally colored films that demonstrated reversible color change when exposed to various moist gases and liquids, achieved by filtrating nanofibrillated cellulose through a porous hydrophobic membrane.

Recently, Li et al.[107] presented a CNC-based schemochrome hydrogel that responds to both pressure and temperature with tunable CLC structure (Figure 8). Through the integration of various interfacial noncovalent interactions, they established dynamic links between the tunable helical pitch of vertically oriented CLC phase and responsiveness of flexible thermosensitive substrates, enabling diverse optical properties and distinctive visual patterns. As the pressure increases, the structural color transitions sequentially from red to orange, yellow, green, and finally blue. When the external pressure is removed, the structural color reverts to its original state within 2 s, showcasing the reversible nature of the structural change (Figure 8c). Furthermore, as temperature increases, the dominant structural color shifts from red to orange, yellow, and ultimately to blue (Figure 8d). The reversible color behavior driven by temperature was further analyzed using the Hue, Saturation, and Value (HSV) color model (Figure 8e), which indicates a direct correlation between H value and temperature. The hydrogel's water content decreases when elevating the temperature from 25 to 55° C, causing *H* value to increase from 9° to 203°, which covers a wide range of the HSV color space (Figure 8f). Hydrogels are employed for on-demand schemochrome patterning, encompassing customizable dual-encryption labels, temperature monitoring, smart digital displays, and intelligent recognition/control systems. This innovative hydrogel, with its dynamic structural color patterns, shows significant potential for the development of next-generation smart optical devices, including anti-counterfeiting systems, intelligent control mechanisms, and temperature monitoring applications.

4.4 | Tension-responsive cellulose-based LCs

The skin functions as a protective barrier, separating the human body from the external environment, and is capable of converting stimuli such as temperature, pressure, tension, and twisting forces into electrical signals. Recently, broad applications in intelligent robotics, medical diagnostics, and wearable technologies have driven researchers to investigate artificial flexible electronic skins that mimic multisensory functionalities.[108] A variety of E-skins capable of sensing external stimuli have been developed through the incorporation of conductive materials, including alloys, ionic liquids, liquid metals, and carbon-based materials.[109] Among these, carbon nanotubes (CNTs) are extensively utilized due to their superior electrical conductivity and mechanical properties.[110] However, many flexible CNT-integrated E-skins depend on external electrical devices for data processing and visualization. Additionally, the single-output electrical signals from these devices often struggle to identify the stimulation site and are susceptible to interference errors. Consequently, there remains a need to develop conductive E-skin that provides visible signal output and can accurately identify the stimulation source. The chameleon's skin can alter its color by adjusting internal periodic arrangements of guanine nanocrystal arrays. To replicate this feature, smart structural color hydrogels have been engineered by integrating responsive polymers with periodic nanostructures that can regulate light propagation.[88n,111] When cellulose CLCs are combined with smart hydrogel scaffolds, the structural colors of the resulting hydrogel can be produced at specific cellulose concentration, with the color changing in response to external stimuli.[86a,88c,88d,88l,112] Based on these, Zhang et al.[113] developed a multifunctional E-skin using LC hydrogel composed of HPC, poly(acrylamide-co-acrylic

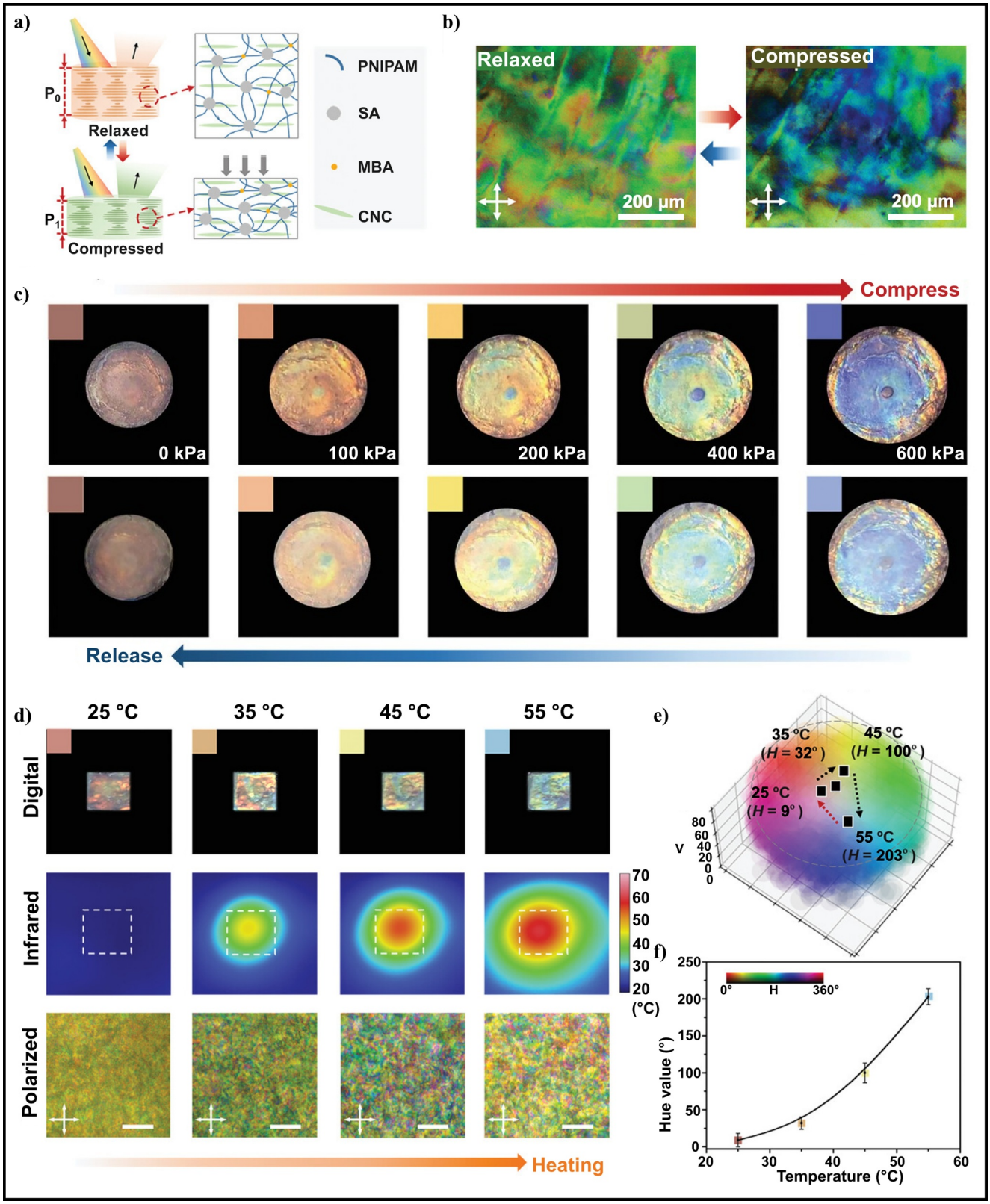

FIGURE 8 (a) Schematic illustration showing changes in nanostructure during relaxation and compression. (b) POM images of the hydrogel in both relaxed and compressed states. (c) Photographs of the sample taken during the compressing and relaxation processes. (d) Photographs, infrared thermal images, and POM images of the sample during the heating process. (e) Thermo-induced color changes illustrated using the HSV color model. (f) The quantitative correlation between H value and temperature. Reproduced with permission.[107] Copyright 2023, John Wiley and Sons. HSV, Hue, Saturation, and Value; POM, polarized optical microscopy.

acid) (PACA),[114] and CNTs (Figure 9). The HPC can form CLC photonic structures, where CNTs boost color saturation and PACA polymerization helps maintain the periodic arrangements. Upon exposure to different stimuli like mechanical pressure, strain, or temperature, the composite hydrogel made of HPC and PACA exhibits noticeable color as a result of volume or internal nanostructure alteration. Furthermore, by incorporating CNTs, the hydrogel can transform these stimuli into electrical resistance signals. That is, the hydrogel E-skin offers quantitative feedback on external stimuli through electrical resistance changes and visually highlights stimulated regions via color changes. This dual-signal sensing capability enables clear interaction and enhanced resistance to interference, making the multifunctional E-skin highly promising for a wide range of applications.

The ability to selectively reflect circularly polarized light across a broad spectral range in response to stimuli is significant from both scientific and technological viewpoints. Qu et al.[115] developed chiral photonic cellulose films capable of selectively reflecting circularly polarized light when exposed to mechanical stimuli (Figure 10a). These chiral photonic cellulose films exhibit superior flexibility, within a strain-at-break of up to 40.8%, which is higher than those have been reported. Moreover, these films exhibit selective reflection of LCP light when bent or subjected to uniaxial tension across the entire visible spectrum. In addition, the films display a reversible response to water vapor (ranging from 10% to 100% RH) across the visible to the near-infrared spectrum. The response to stimuli is facilitated by the tunable helical structures based on supramolecular chemistry. This research presents an effective method for the strategic design of materials in response to multiple stimuli, offering a flexible soft material platform for large-scale applications in camouflage and security technologies. Xu et al.[116] reported luminescent CNC shape-memory polymers (CNC-SMPs) that exhibit mechanically triggered circularly polarized light emission. Through adjusting the swelling ratio of the CNC film precursor, they established a controlled polymerization method to create CNC-SMPs with adjustable structural color. When the materials were heated above their glass transition temperature (T_g), mechanical stress was applied to compress the cholesteric structures. Through hot-pressing and thermal recovery, the CNC-SMPs demonstrate reversible on/off circularly polarized light emission (Figure 10b). Jia et al.[4c] reported a chiral photonic crystal film that exhibits significant rigidity and superior flexibility, capable of enduring multiple mechanical deformation (Figure 10c). Without destroying cholesteric structure, the film can bear a strain of nearly 50%, which exceeds

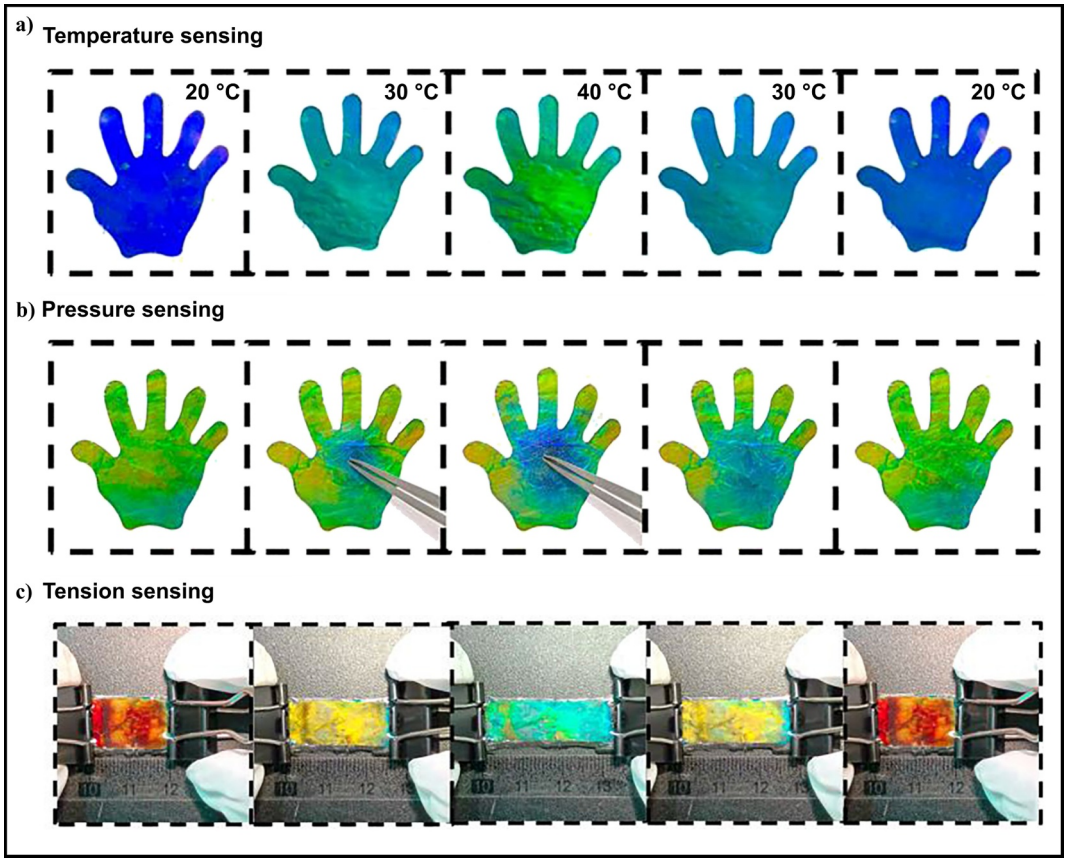

FIGURE 9 (a) Temperature sensing evaluation of the E-skin. (b) Pressure and (c) tension sensing evaluation of the E-skin. Reproduced with permission.[113] Copyright 2020, National Academy of Sciences.

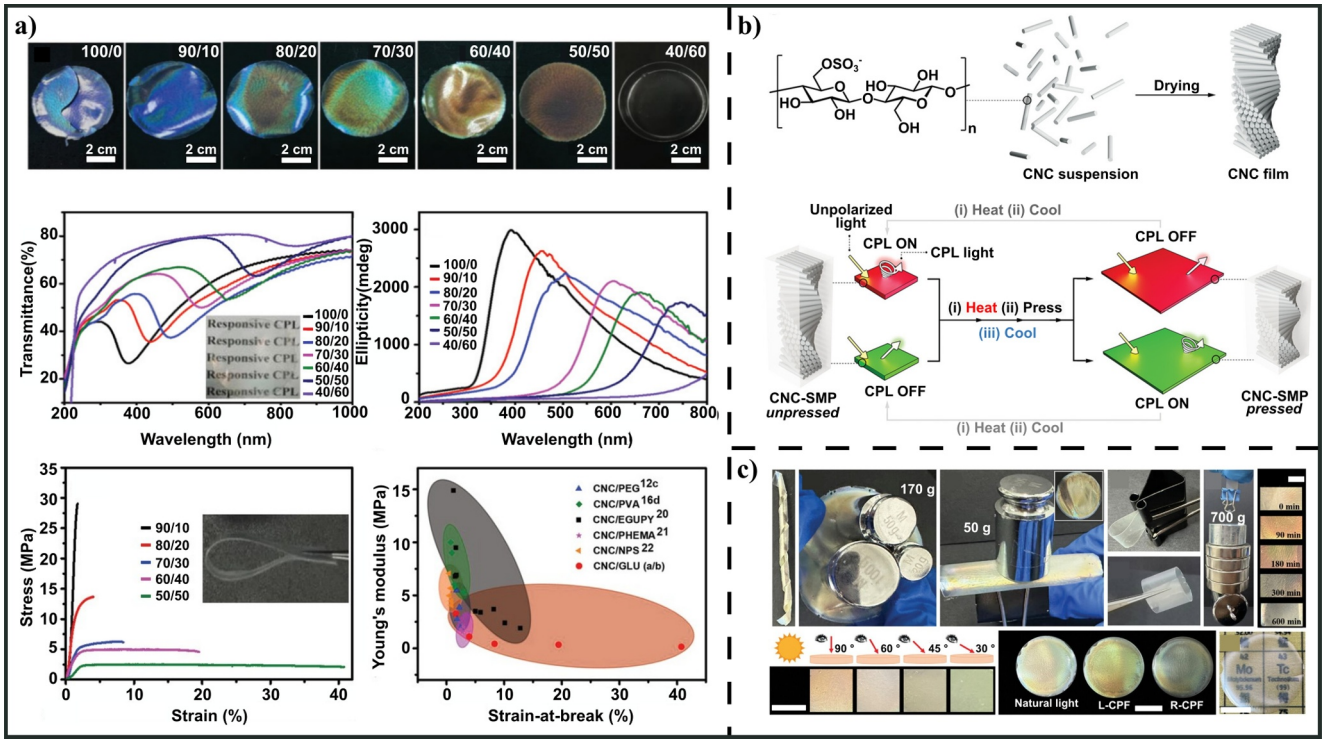

FIGURE 10 (a) Photographs depicting chiral photonic cellulose film with varying GLU content, corresponding transmittance spectra, CD spectra, and stress–strain curve of CNC/GLU. Reproduced with permission.[115] Copyright 2019, John Wiley and Sons. (b) Diagrams illustrating the chemical structure and cholesteric structure of CNC film. Reproduced with permission.[116] Copyright 2023, John Wiley and Sons. (c) Twists, pressure-proof, bends, rolls, and tensile properties of the photonic crystal film. Reproduced with permission.[4c] Copyright 2024, John Wiley and Sons. CD, circular dichroism; CNC, cellulose nanocrystal; GLU, glucose.

most cellulose-derived materials. These photonic crystal materials combine outstanding mechanical properties with unique optical performance, with their film colors spanning the entire visible region by tuning the photonic band gaps (PBGs). As a result, these materials can be utilized in security and anti-counterfeiting applications due to their eco-friendly, cost-effective, non-destructive, and user-friendly authentication properties.

4.5 | Electricity-responsive cellulose-based LCs

CNCs possess unique properties that enable their applications in high-value functional nanostructured materials. Integrating anisometric dopants, such as plasmonic gold nanorods, into the cholesteric structure is capable of improving the control over their orientation and positional order.[117] However, self-assembled structure often exhibits weak long-range order, leading to polydomain structure with misalignment that produces a rainbow-like appearance rather than distinct optical effect.[118] Different approaches and stimuli have been investigated to enhance the long-range order of cholesteric CNC suspensions, but strong hydrodynamic shear often disturbs the cholesteric arrangement, transforming it into a nematic structure.[119] Ličen et al.[11b,120] showed that applying mild circular shear to a drying suspension in a round container improves the local vertical alignment of the cholesteric structure. However, a gradual distortion of helicoidal ordering was observed near the edge. Additionally, extensive research has been conducted on the alignment of colloidal LCs under the influence of electric or magnetic field.[121]

Frka-Petesic et al.[84d] demonstrated that an electric field can effectively manipulate the iridescent characteristics of CNCs in an apolar solvent (Figure 11a), enabling precise regulation of helical pitch, macroscopic sample uniformity, and structural color. The influence of an electric field on the alignment and periodicity of cholesteric phase was evaluated through visual iridescent effect and laser diffraction analysis. Specifically, the sample was positioned inside a vertical glass capillary fitted with metal electrodes connected to a high AC voltage source. A white light was placed slightly off-center in the vertical plane behind the sample. At a low electric field, the light intensity increases noticeably, followed by a red shift in color. As the electric field increases, the color shifts to a scattering white and eventually disappears. However, under a strong field, it becomes uniform, signifying the alignment of the CNCs parallel to the applied field and a transition to a paranematic phase. Fernandes et al.[11b] fabricated a novel cellulose-based photonic structure that can reflect both RCP and LCP light, whose reflection can be tuned by temperature and electric field (Figure 11b). By using an LC as an anisotropic half-wave retardation plate,

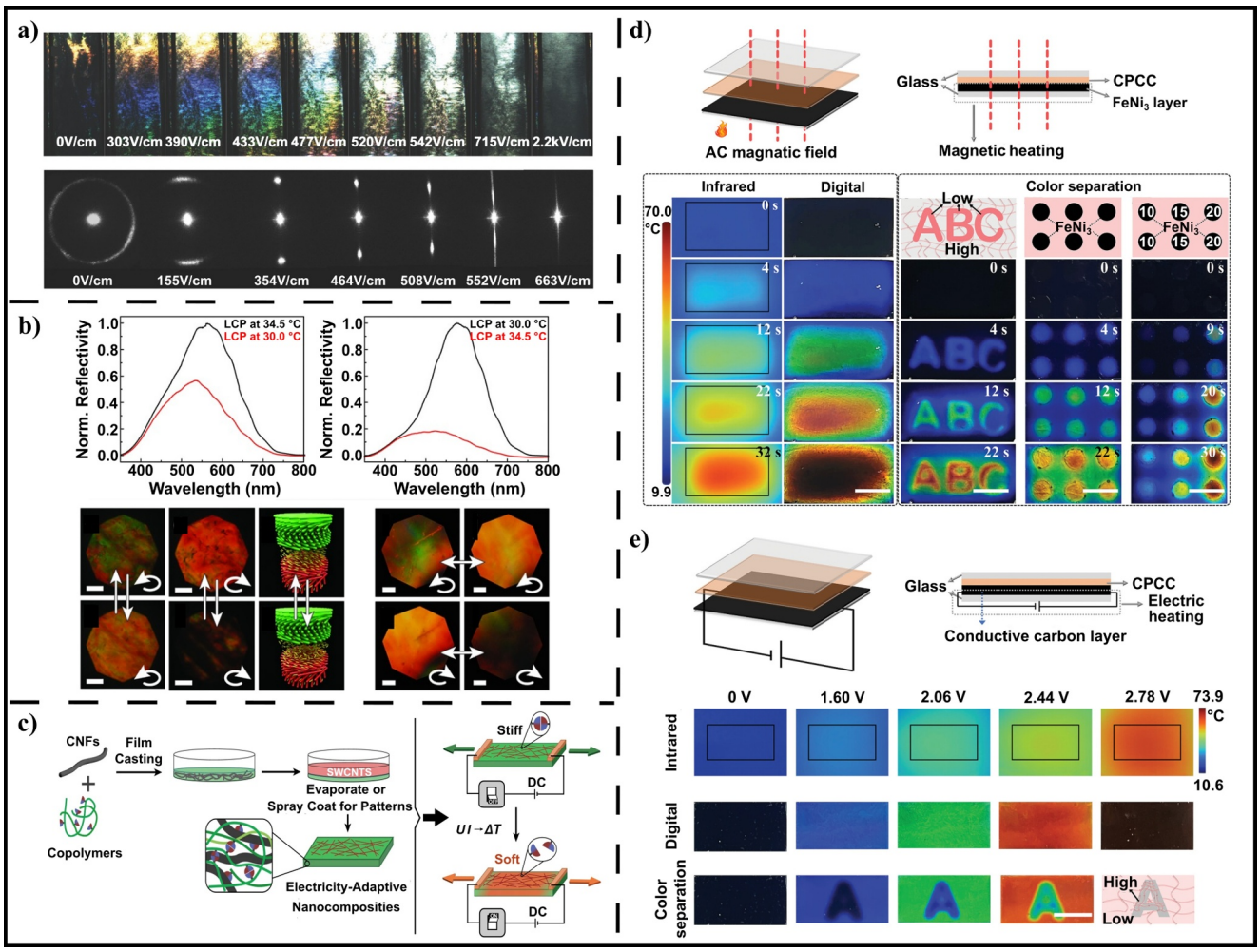

FIGURE 11 (a) Iridescence changes of a cholesteric polydomain sample under electric field (top) and the formation of the laser diffraction pattern as the electric field increases (bottom). Reproduced with permission.[84d] Copyright 2017, John Wiley and Sons. (b) Thermal switching of reflected LCP and RCP channels in chiral CNC/LC films. Reproduced with permission.[11b] Copyright 2016, John Wiley and Sons. (c) Electrical switching of bioinspired nanocomposites based on CNFs and hydrogen-bonded polymers. Reproduced with permission.[122] Copyright 2021, Springer Nature. Design and performance of magneto-thermochromic (d) and electro-thermochromic (e), and devices based on CPCC. Reproduced with permission.[125] Copyright 2024, John Wiley and Sons. CNC, cellulose nanocrystal; CNFs, cellulose nanofibrils; CPCC, cholesteric phase cellulose composites; LC, liquid crystal; LCP, left-handed circularly polarized; RCP, right-handed circularly polarized.

the reflected RCP light and LCP light channels can be controlled by changing the birefringence, which can be induced by temperature variations. The reflected RCP and LCP can be affected by the nematic-to-isotropic transition (T_{NI}). Above T_{NI}, the red reflection of LCP light maintains, while the reflection of RCP light becomes colorless. Notably, the wavelength of the reflected LCP light increases when the temperature exceeds T_{NI}. The wavelength of light reflecting along the cholesteric axis can change due to two factors: the average refractive index of the phase and the pitch. A decrease in the refractive index of the material causes the pitch of cholesteric phases to increase due to the isotropic liquid between layers. The system's birefringence can be regulated by applying an electric field to the stimuli-responsive LC layer. The effect of the electric field and temperature is similar: while the RCP light disappears, the reflection in LCP light channel shifts towards large wavelength. The application of an electric field prompts the nematic molecules to align along the direction of the field due to the positive dielectric anisotropy.

Jiao et al.[122] incorporated electrical switching into bio-inspired nanocomposites, which demonstrate mechanical property regulation under low direct current (DC) conditions (Figure 11c). The application of DC induces significant electrothermal softening by initiating the dynamization and disruption of thermo-reversible supramolecular bonds. The modified mechanical characteristics can be reversibly modified through activation and deactivation of power. This straightforward and versatile approach advances the development of bioinspired nanocomposites, enabling applications in structural materials, adaptive damping, and soft robotics. Cellulose has garnered considerable attention across multiple fields owing to its widespread availability, biodegradability, non-toxicity, and ease of processing.[116,123] HPC can

spontaneously form CLC structures,[85,113] which selectively reflect light and exhibit vivid structural colors.[107] Inspired by chameleons, a variety of external stimuli, such as mechanical forces,[124] heat,[91] electricity,[84d] and solvents,[91] have been employed to modulate the pitch of CLC structures, thereby altering the structural color. Achieving consistent coloration at ambient temperature and facilitating multicolor separation at elevated temperature is highly desirable. However, the development of stable photonic devices capable of inducing multicolor separation through straightforward and easily obtainable stimuli, like low voltage or weak magnetic field, remains a challenge for practical applications. Wen et al.[125] proposed a flexible strategy for achieving multicolor separation in cholesteric phase cellulose composites (CPCC) (Figure 11d,e). The CPCC was synthesized by combining a high-concentration self-assembled HPC with a cross-linked poly(acrylic acid-acrylamide) (P(AA-AM)) network. By modulating the cross-linking density of P(AA-AM) in CPCC, thermally induced multicolor separation was achieved, transitioning from a uniform color at room temperature to a multicolor pattern at elevated temperature. Moreover, by leveraging the electric heating effect of conductive carbon oil, the multicolor separation was achieved under low voltage by incorporating $FeNi_3$ nanoparticles into CPCC. The multicolor separation effect was improved by the pixelated distribution of $FeNi_3$ nanoparticles and the variation of the concentration within each pixel. Additionally, thermochromic, electro-thermochromic, and magneto-thermochromic properties can be integrated into CPCC, enabling advanced multilevel information encryption.

4.6 | Magnetic force-responsive cellulose-based LCs

A magnetic field has been utilized to achieve uniform alignment of lyotropic CLC phase in biopolymers, resulting in a consistent global orientation and optical appearance. Barhoumi Meddeb et al.[126] demonstrated that the application of a magnetic field can alter the anisotropic alignment of cholesteric CNCs in both aqueous and non-aqueous suspensions. Kim et al.[127] demonstrated that the left-handed cholesteric CNC films, featuring homeotropic concentric helix orientations within planar textures, can be achieved by the self-assembly of CNCs directed using a local radial magnetic field (Figure 12a). These cholesteric CNC films demonstrate left-handed circular polarization characteristics and transform spontaneous emission into right-handed CPL across the film's surface and its lateral surfaces due to the PBGs. The Fe_3O_4 nanoparticles spontaneously form particle-like clusters, which are organized into linear assemblies that grow and align along the magnetic field's direction. Simultaneously, birefringence accompanied by fingerprint textures appears, evolving into ellipsoidal factoids and eventually merging into cholesteric fragments through tactoid coalescence. This study marks a significant advancement in the development of self-assembled chiroptical materials with complex polarization properties, which are crucial for photonic applications. Li et al.[128] demonstrated that weak, patterned magnetic field gradients can generate intricate optical effects by spatially organizing needle-shaped, magnetically modified CNCs (Figure 12b). The formation of thin films with an optical pattern containing both chiral and achiral regions are associated with vortices induced by local magnetic gradient during the flow of the LC suspension. The local tracking of the flow direction of the magnetically modified nanocrystals reveals the interaction between evaporation and field-driven localized flow, which influences the formation of twisted structure within the magnetically generated vortices. Frka-Petesic et al.[129] demonstrated that neodymium (NdFeB) magnet can effectively control the alignment of cholesteric domains, enabling colored CNC films with precise manipulation of their optical characteristics (Figure 12c). This is accomplished by evaporating the suspension near NdFeB magnets, where the magnetic field induces a long-range ordering in the cholesteric phase. Modifying the spatial arrangement of the magnet relative to the drying suspension can improve the alignment uniformity of the cholesteric axes, resulting in large, uniform films with accurate orientation control. This straightforward but highly effective approach opens up new opportunities for designing visual properties of iridescent films, enabling textures from metallic to pixelated or matte finishes and advancing development of sustainable photonic pigments for use in coatings, cosmetics, and security labels.

5 | OPTICAL PROPERTIES OF CELLULOSE-BASED LCs

5.1 | Circularly polarized light modulation

The regulation of light is essential for applications like broadband reflectors and optical diodes.[130] Photonic crystals, characterized by periodic variations in dielectric properties, demonstrate significant potential in controlling light propagation owing to their PBGs.[87b,129,131] In the periodic structure, certain light wavelength will be forbidden from propagating, resulting in the PBGs.[132] CPL describes the differential emissions of left- and RCP light from chiral luminescent clusters or systems in an excited state.[133] Basically, helical nanostructure-based CLCs, acting as chiral templates, represent the most widely employed approach for generating tunable CPL with large g_{lum} values.[134] Stimuli-responsive LC-based soft materials demonstrate selective reflection of circularly polarized light with the same handedness as the LC helical axis.[135] Combining achiral luminescent dopants with CNCs provides a straightforward approach to develop CPL composite films, serving as a practical alternative to chiral luminophores.[136] CNC-emitter films function as a "host-guest" dual system, with luminescent materials embedded within the left-handed cholesteric CNCs. Achiral emitters, such as rare earth doped nanoparticles,[137] organic luminophores,[138] carbon

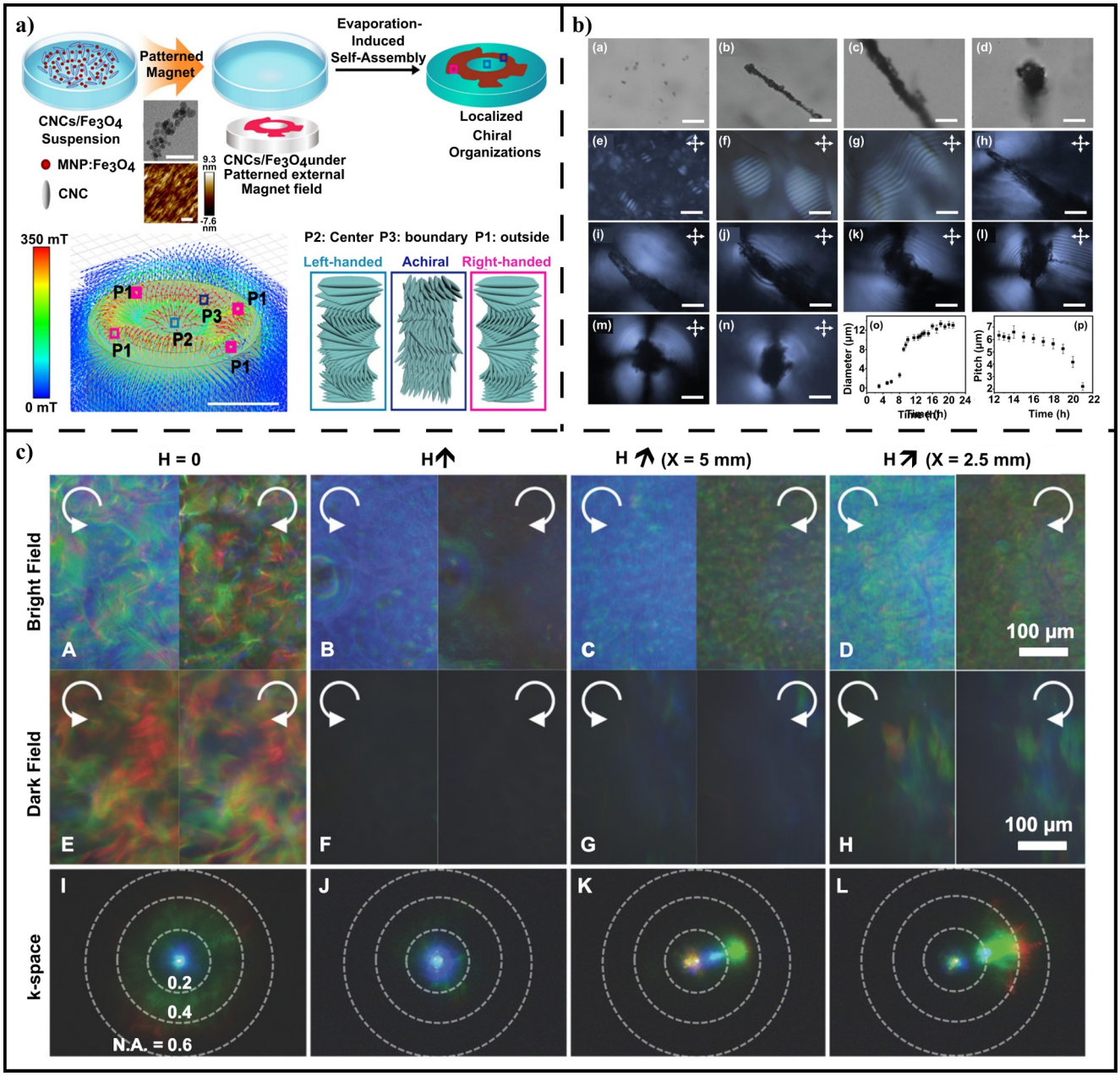

FIGURE 12 (a) Schematic illustration of the process for regulating localized chirality inversion in self-assembled CNCs using magnetic field gradient patterns. Reproduced with permission.[127] (b) Monitoring the magnetic field-directed self-assembly of CNC-Fe_3O_4 using POM. Reproduced with permission.[128] Copyright 2022, John Wiley and Sons. (c) POM images of prepared films under different magnetic fields. Reproduced with permission.[129] Copyright 2017, John Wiley and Sons. CNCs, cellulose nanocrystals; POM, polarized optical microscopy.

dots (CDs),[139] quantum dots,[38a] and quantum rods[140] have been utilized as luminescent guests. CNCs exhibit significant optical iridescence and display a dynamic interaction between structures, photonic properties, and functionalities.[11b,14,95] A range of composite films has been produced by integrating CNCs with achiral luminophores like dyes,[138a] or lanthanide complexes,[141] allowing for right-handed CPL emission with elevated g_{lum} values. These composite materials can be utilized in polarization-based anti-counterfeiting and cancer detection.[142] Jia et al.[32a] employed self-assembled CNCs as chiral templates to produce CPL films (Figure 13a). By manipulating the PBGs, the resulting films display a strong CPL signal with excellent mechanical flexibility. In addition, the films achieve a remarkable ultimate strain of 19%, surpassing most CNC-based chiral luminescent assemblies while maintaining CPL activities, making it a promising material for optical sensors and wearable devices. Duan et al.[143] developed a novel dual PBG structure using CNC/fluorescent carbon quantum dots films and CNC films, enabling real-time control over intensity, wavelength, and direction of CPL emission by simply tailoring the physical position of the

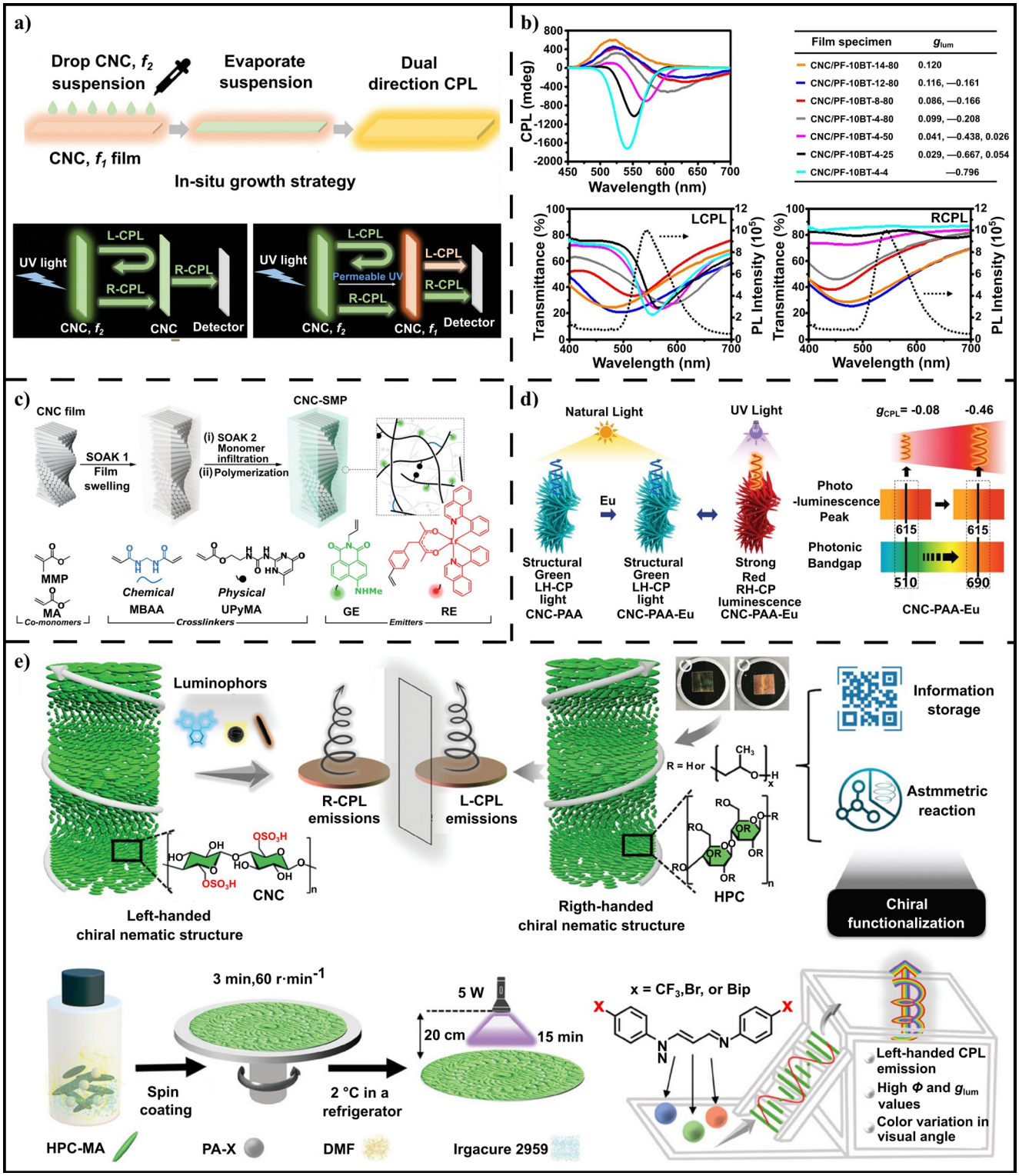

FIGURE 13 (a) Preparation of dynamic and switchable dual-direction CPL optical films. Reproduced with permission.[32a] Copyright 2024, John Wiley and Sons. (b) CPL spectra, g_{lum} values, and transmission spectra of CNC films probed by LCP light and RCP light. Reproduced with permission.[144] (c) Preparation of luminescent CNC-SMP. Reproduced with permission.[116] Copyright 2023, John Wiley and Sons. (d) CNC–PAA–Eu composite exhibits visible color change, transitioning from green left-handed CPL to red right-handed CPL emission. Reproduced with permission.[141b] Copyright 2021, John Wiley and Sons. (e) Conceptual design of integrating aggregation-induced emission molecules into chiral photonic cellulose films to develop circularly polarized light-emitting materials. Reproduced with permission.[147] Copyright 2024, John Wiley and Sons. CNC-SMP, cellulose nanocrystal-based shape-memory polymers; CPL, circularly polarized luminescence; LCP, left-handed circularly polarized; PAA, polyacrylic acid; RCP, right-handed circularly polarized.

films. This advancement improves the precision of manipulating circularly polarized signals compared to those methods involving chemical or photonic stimulation.

Tao et al.[144] showed that the self-assembled CNC films reflect circularly polarized light, reaching a peak reflectivity of 68%. These films are capable of converting spontaneous photoluminescence into both RCP and LCP luminescence, with $|g_{lum}|$ values of 0.796 and 0.120, respectively (Figure 13b). The chiroptical characteristics arise from a left-handed cholesteric structure, featuring a nematic-like phase that functions as a half-wave retarder between two PBG layers. The PBG layers are inherently incorporated into the left-handed helical structure via rapid gelation of CNC colloidal suspension. The chiroptical features can be finely tuned by modifying the evaporation temperature, concentration, and properties of the CNC suspension. So far, scientists have incorporated luminophores, including organic small molecules,[138b] CDs,[30b,139a] quantum dots,[5b,145] and upconversion nanoparticles,[146] into cholesteric CNC films to generate right-handed CPL emission with notable $|g_{lum}|$ values. Achieving high $|g_{lum}|$ depends on the matching of the PBGs of CNCs and the emission bands of the luminophores. The PBGs of CNC films exhibit strong sensitivity to variations in humidity and solvent conditions, which makes them excellent materials for CPL sensors.[141b,146] However, the CNC films are fragile and exhibit limited response to conditions other than the humidity and different solvents. Xu et al.[116] demonstrated that CNC-based shape-memory polymers (CNC-SMPs) incorporating luminescent elements can yield mechanically responsive CPL (Figure 13c). By modulating the PBGs of CNC-SMPs, it is possible to accurately control CPL emission with different wavelengths and elevated g_{lum} values. The CPL emissions can be reversibly controlled by hot-pressing the luminescent CNC-SMPs and then restoring them with heat. The pressure-sensitive PBGs allow for pressure-responsive CPL with tunable g_{lum} values.

Kim et al.[141b] developed biosynthetic light-emitting adhesive materials composed of cholesteric CNC–polyelectrolyte complexes, which demonstrate strong adhesion to both hydrophilic and hydrophobic substrates (Figure 13d). By incorporating europium doping, they achieved intense and dynamic photoluminescence with high g_{lum}, while preserving adhesive strength and iridescent characteristics. The photoluminescence can be suppressed by exposure to volatile acetone vapor or liquid and rapidly restored to its original state upon drying. These unique features—universal adhesion, improved and dynamic photoluminescence, and tunable CPL—make these light-emitting bio-adhesives particularly suitable for applications in security optical coding, covert communication, and biochemical sensing, especially in wearable stickers and prints. Huang et al.[147] developed a novel system that combines aggregation-induced emission molecules with optical stability into cholesteric HPC materials, achieving robust left-handed CPL emission (Figure 13e). This system was developed through a helical co-assembly method, embedding N-(3-(phenylamino) allylidene) aniline hydrochloride (PA) derivatives into the cholesteric methacrylate-functionalized HPCs, which were subsequently dispersed in dimethylformamide (DMF). By employing DMF solvent as the medium, a uniform hybrid with remarkable iridescence and a well-organized helical structure in HPC−PA film is formed through photo-crosslinking. The obtained photonic film exhibits remarkable flexibility, excellent mechanical strength, and color changes that depend on the viewing angle. Furthermore, the film shows a strong L-CPL emission with a high g_{lum} value of 0.51. Importantly, the versatile modification of PA skeleton plays a pivotal role in multicolored emission. Moreover, the film shows outstanding resistance to different organic solvents and maintained stability in water for over 3 months. These chiral photonic materials based on HPC hold significant potential for applications in fields such as chiral molecular sensing, information storage and encryption, and asymmetric catalysis.

Sun et al.[148] fabricated an HPC film by incorporating a curing agent, hydroxyethyl methacrylate (HEMA), into the initial HPC solution, whereas a CNC film was produced by mixing glucose (GLU) with a CNC suspension (Figure 14). The chiroptical characteristics of these cellulose-based films exhibit symmetry: the right-handed cholesteric HPC/HEMA film allows the transmission of L-CPL (Figure 14a), and the left-handed cholesteric CNC/Glu film permits the transmission of R-CPL (Figure 14b). Both films display high g_{lum} values, making them ideal options for inducing chirality in azobenzene polymers. Integrating HPC and CNC films with opposite handedness into a single material can achieve a switchable circularly polarized light emitter (CPLE). However, switchable CPL is not achievable by directly combining these two films. Therefore, a Janus-structured CPLE was engineered by placing a luminescent layer between two cellulose-based films (Figure 14c). The emitter can be switched between L-CPL and R-CPL through the modulation of the emission mode. Furthermore, the chiral helices in azobenzene polymer, which incorporate side chains with diverse polar groups, were fabricated using this highly efficient CPLE (Figure 14d). The chirality of the polymer helices can be accurately regulated by adjusting the luminescent modes of the CPLE. This research opens up new possibilities for the design and construction of novel cellulose-based CPL-active materials.

5.2 | Circular polarized phosphorescence

Stimulus-responsive CPL materials have attracted significant attention for the development of advanced smart photonic materials.[143] Particularly, room temperature phosphorescence (RTP) materials have been extensively studied for applications in anti-counterfeiting and optical imaging.[149] Nevertheless, most RTP materials suffer from short lifetimes due to the quenching of their triplet excited states by atmospheric oxygen, which limit their practical applications.[145] Organic RTP materials possess unique

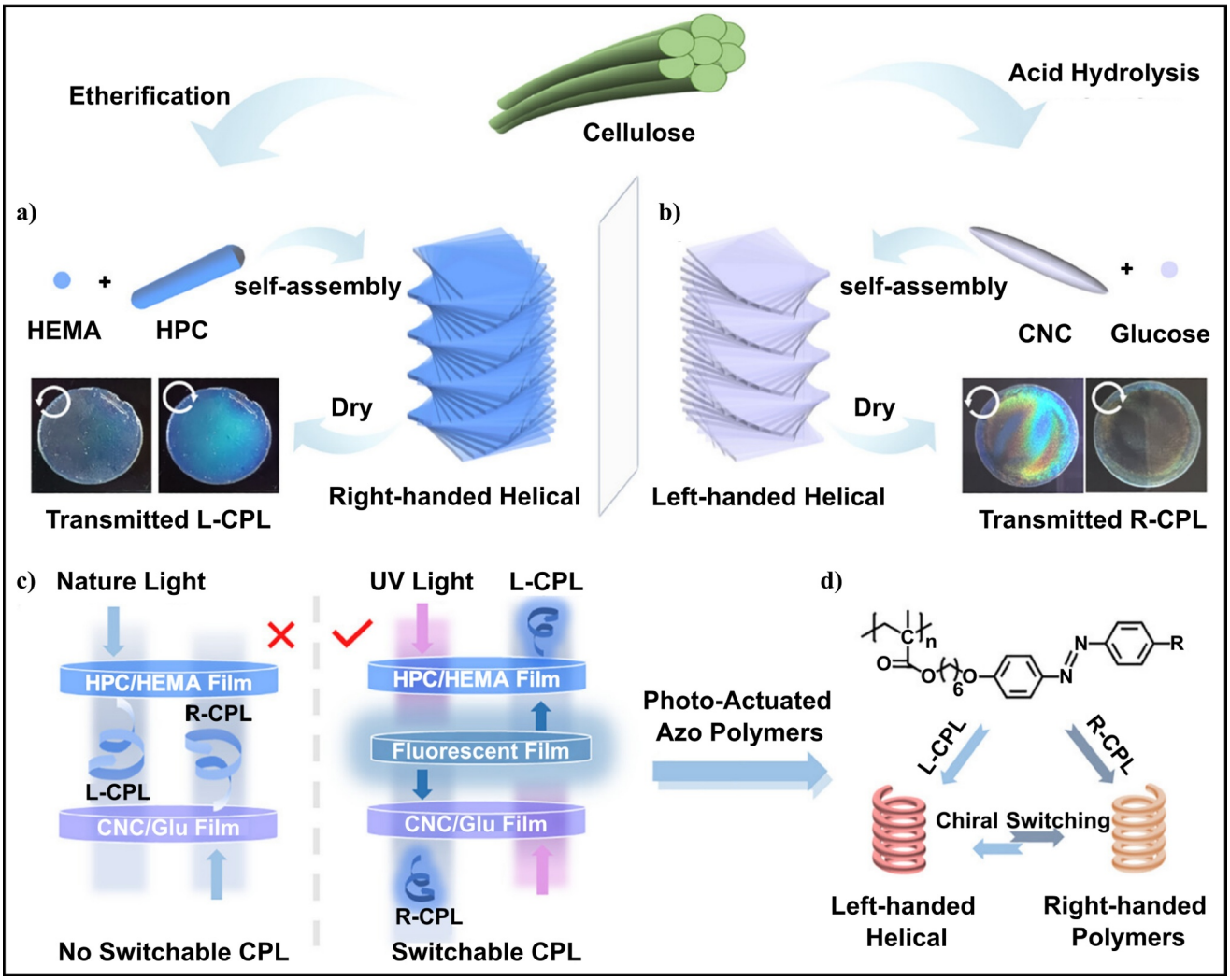

FIGURE 14 (a) Schematic illustration of right-handed helical structure of HPC/HEMA film and the formation of L-CPL. (b) Schematic illustration of left-handed helical structure of CNC/Glu film and the generation of R-CPL. (c) Schematic illustration of the CPLE with a Janus structure that emits L- and R-CPL. (d) CPLE for the photoinduced supramolecular chiral helices of azobenzene polymer. Reproduced with permission.[148] Copyright 2024, John Wiley and Sons. CNC, cellulose nanocrystal; CPLE, circularly polarized light emitter; GLU, glucose; HPC/HEMA, hydroxypropyl cellulose/hydroxyethyl methacrylate.

characteristics such as large Stokes shifts, extended emission lifetimes, and excellent processability,[149d,150] making them particularly appealing for multifunctional optical applications. Recently, circularly polarized room-temperature phosphorescence (CP-RTP) materials, which integrate RTP[151] and CPL, have become a research hotspot for scientists due to their long-lived lifetimes and the ability to generate multiple optical signals that remain observable even after the excitation source is turned off for. Yu et al.[138c] adjusted the intensity and wavelength of CPL emission by controlling the fluorescence and chirality. The CPL composite films are fabricated through the co-assembling of fluorescent polymer and partially desulfurated CNCs, leading to the formation of left-handed cholesteric structure in the composite films. These films exhibit sensitivity to different stimuli, such as acid/base conditions, water content, and polar solvents. Additionally, the CPL composite films exhibit tunable and reversible responsiveness, highlighting their significant potential for advancing cutting-edge information and display technologies.

Zheng et al.[138a] demonstrated that cellulose films with left-handed helical arrangements naturally exhibit circular polarization, resulting in PBG-based CPL with enhanced $|g_{lum}|$ values, well-defined handedness, and tunable wavelength. These cellulose films can convert incident light ranging from near-UV to near-IR into passive L-CPL and R-CPL, with handedness dependent on the viewing side, achieving a $|g_{lum}|$ value of up to 0.87. Xu et al.[30b] used the EISA method to develop hybrid chiral photonic films that exhibit both dual CPL and CP-RTP (Figure 15a). CDs serve as the luminescent guest, whereas CNCs and polyvinyl alcohol are utilized to construct a photonic host matrix with adjustable properties. The matrix can stabilize triplet state excitons by forming hydrogen bonds with the CDs,

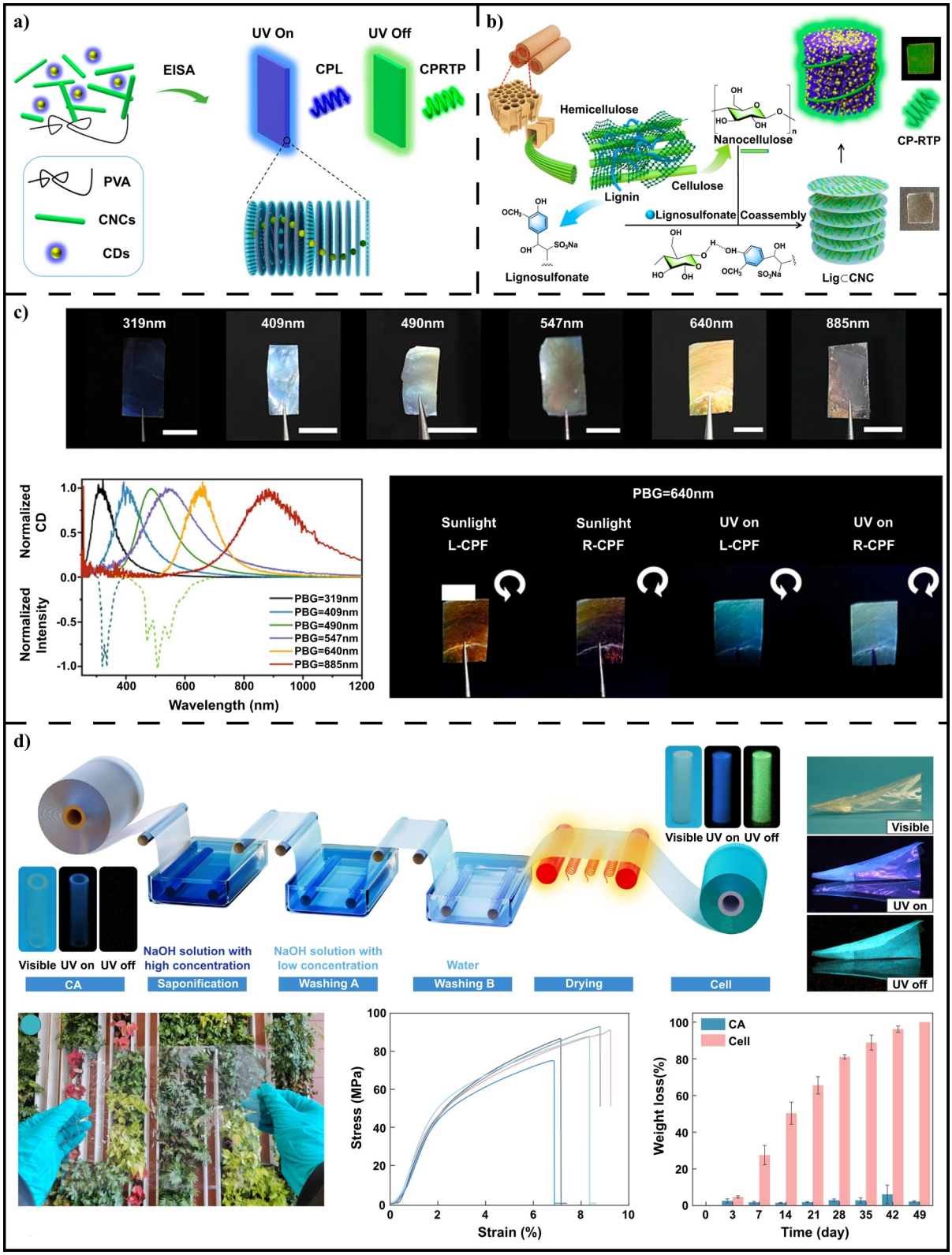

FIGURE 15 (a) Schematic illustration of the process for the fabrication of sustainable CP-RTP. Reproduced with permission.[30b] Copyright 2020, American Chemical Society. (b) CNCs and phosphorescence-active lignosulfonate collaboratively to produce phosphorescent chiroptical films. Reproduced with permission.[152] Copyright 2024, Springer Nature. (c) Images of NP-CNC films. Reproduced with permission.[153] Copyright 2024, Elsevier. (d) Large-scale preparation of full-color CPL films. Reproduced with permission.[154] CNCs, cellulose nanocrystals; CPL, circularly polarized luminescence; CP-RTP, circularly polarized room-temperature phosphorescence; NP, naphthalene.

effectively suppressing nonradiative relaxation. Meanwhile, the cholesteric structure protects triplet excitons generated via the intersystem crossing process, enabling their relaxation in a chiral environment. Thus, this hybrid nanostructured material emits CPL under UV exposure and exhibits CP-RTP upon cessation of the excitation light. Cao et al.[152] developed biobased thin films that demonstrate both CPL and RTP (Figure 15b). Phosphorescence-active lignosulfonate biomolecules were co-assembled with CNCs in a chiral framework. The lignosulfonate adopts the chirality induced by CNCs within the films, producing CP-RTP with a g_{lum} value of 0.21 and a phosphorescence lifetime of 103 ms. In contrast to traditional organic phosphorescence materials, this chiral-phosphorescent system demonstrates remarkable stability, maintaining phosphorescence without significant degradation even under extreme chemical conditions. Meanwhile, the luminescent films exhibit water resistance and durability in humid environments. This environmentally friendly, bio-based CPP system holds significant potential for advancing applications in information processing and anti-counterfeiting technologies.

Wang et al.[153] successfully synthesized CP-RTP materials by embedding polycyclic aromatic hydrocarbon-doped polymethyl methacrylate into CNC films (Figure 15c). The tunable $|g_{lum}|$ reaches the maximum value of 0.49, with an afterglow lasting up to 8 s. The intensity, wavelength, and chirality of CP-RTP and circularly polarized fluorescence emission are controlled by tuning the PBGs of the CNCs. The hybrid CNC films exhibit structural color, phosphorescence, and CP-RTP behaviors, making them promising candidates for multi-channel data storage in anti-counterfeiting applications. These findings highlight their potential for diverse photonic applications, including chiral polarizers, information security, and 3D displays. Jin et al.[154] developed a straightforward method for producing CP-RTP materials with tunable structural color, excellent flexibility, and biodegradability, achieving a high g_{lum} value of 0.16 by optimizing hydrogen-bonding interactions within cellulose chains (Figure 15d). Thes cellulose-derived CP-RTP materials hold great promise for advancing applications in optical devices, anti-counterfeiting, and visual sensing technologies.

6 | APPLICATIONS

6.1 | Gas detection

Traditional CNC films derived from biomass typically encounter challenges such as limited sensitivity and slow response time owing to their dense structure. To address this issue, Liu et al.[155] utilized a unidirectional interlayer freezing-photopolymerization method to introduce porous structure into CNC photonic films, with vivid structural color maintained (Figure 16a–c). CNCs are integrated with photopolymer polyethylene glycol diacrylate and organized into a periodic spiral pattern, which forms the foundation for color generation. During the directional freezing process, ice crystals in the CNC suspension grow unidirectionally within the interlayer space of the arranged CNCs, preserving the original structure and their cholesteric color properties. The resulting porous CNC photonic films demonstrate a significant color change and quick responsiveness to different solvents. This approach represents a significant advancement in the development of sustainable and highly sensitive sensor technologies. Song et al.[104] developed a controllable technique to produce color patterns on solid substrates (Figure 16d). The color can be adjusted by changing the assembly of the CNCs solution during the dip-and-pull process. By adjusting the pulling speed, the film thickness could be adjusted from 100 to 300 nm, producing different color films across the visible spectrum. Previous studies report that adding CNCs to polysulfone ultrafiltration membranes significantly improves their anti-fouling performance, pure water flux, contaminant removal efficiency, and mechanical properties.[156] However, these methods typically involve a low incorporation of CNCs, which may leach or detach from the membrane surface over time. Xie et al.[157] developed an eco-friendly approach to produce anti-fouling ultrafiltration membranes by modifying the surface of sulfonated polysulfone (SPSF) membrane with CNCs (Figure 16e). The ultrafiltration membrane was fabricated by filtering a CNC suspension through SPSF ultrafiltration membrane. The membrane achieved nearly 100% retention of pollutants with particle size larger than 10 nm and showed almost double the water flux compared to the SPSF membrane under sewage filtration conditions. The application of CNCs for surface modification on SPSF ultrafiltration membranes significantly enhances the anti-fouling ability, providing a valuable benchmark for enhancing ultrafiltration membrane performance.

6.2 | Anticounterfeiting

Currently, most advanced anti-counterfeiting labels aim to encode information using stimulus-responsive luminescent or structural color patterns, including quantum dots,[158] perovskite nanocrystals,[159] time-dependent phosphorescence materials,[160] and lanthanide luminescence.[161] Developing a cost-effective, user-friendly, and intricate anti-counterfeiting method that enables convenient authentication remains a significant challenge. Zhang et al.[141a] employed a co-assembly approach to produce eco-friendly, large-scale, quadruple-level chiral luminescent materials (CNC/PEG–Eu) by integrating lanthanide complexes into a poly(ethylene glycol) matrix and CNC films (Figure 17a). The films exhibit full-spectrum structural color and tunable fluorescence through control of the cholesteric structure. The chiro-optical behaviors, shifting from azure to khaki, could be controlled using a polarizing filter at specific rotation angles. The CNC/PEG–Eu film was self-assembled into a hollow mold, and once fully dried, the patterned photonic labels were transferred onto the substrates. A glass slide was coated with an adhesive plastic film featuring a

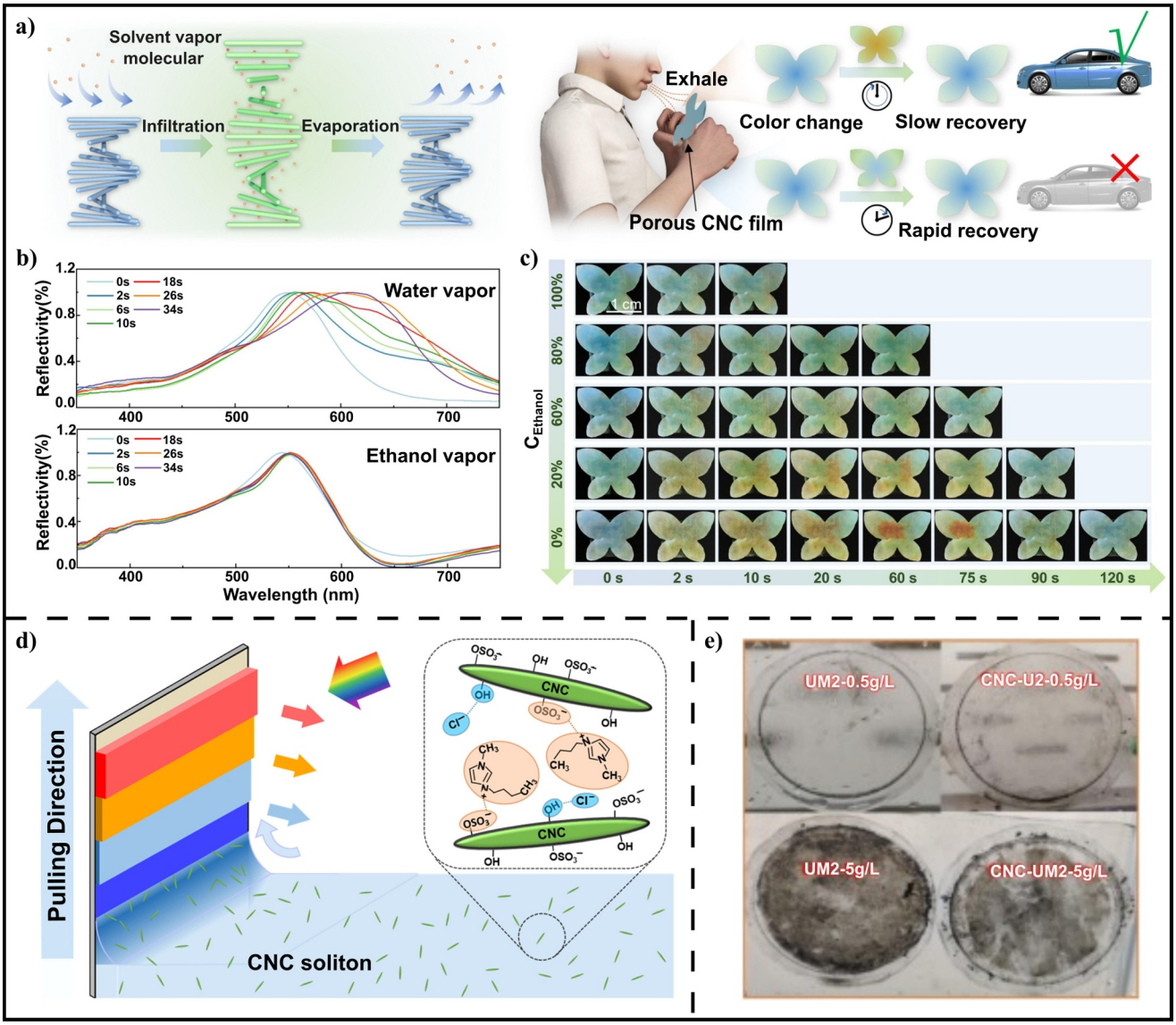

FIGURE 16 (a–c) Application in visualized alcohol detection. Reproduced with permission.[155] Copyright 2025, Elsevier. (d) Schematic illustration depicting the fabrication of CNC-based films on solid substrates using ionic liquids. Reproduced with permission.[104] Copyright 2018, American Chemical Society. (e) Photos of contaminated membranes. Reproduced with permission.[157] Copyright 2025, Elsevier. CNC, cellulose nanocrystal.

hollow "DICP" pattern. A CNC/PEG–Eu suspension was spread onto the exposed film. Following a 6-h drying period and the removal of the mask, a blue "DICP" layer was formed. This anti-counterfeiting system demonstrates characteristics such as responsive photoluminescence, four-color versatility, flexibility, and solvent resistance.

PA is a unique and efficient AIE-active skeleton molecule that functions via halogen bond interactions, which exhibits remarkable photophysical properties in contrast to conventional AIE systems, such as intense solid-state luminescence, high quantum efficiency, and good scalability. HPC was esterified with methacrylic anhydride (HPC-MA). The unique optical properties of poly(HPC-MA)/PA (HMP) allow for the potential applications in anticounterfeiting labels, which feature three different optical states. The HMP-Br precursor easily adheres to different substrates, facilitating the simple self-assembly of HMP-Br composites via photo cross-linking, making it suitable for use on various substrates like wood, glass, and polyethylene terephthalate (Figure 17c).[147] For patterning the letter Y on a complex matrix surface, like a shirt, the "openwork coating printing" method was utilized. Under L-CPL illumination, the label becomes dark, while it turns brighter when exposed to R-CPL. Furthermore, the light-modulating properties of chiral photonic CNC films, along with the integration of a QR code, highlight the potential of chiroptical materials for product authentication and security (Figure 17d).[144]

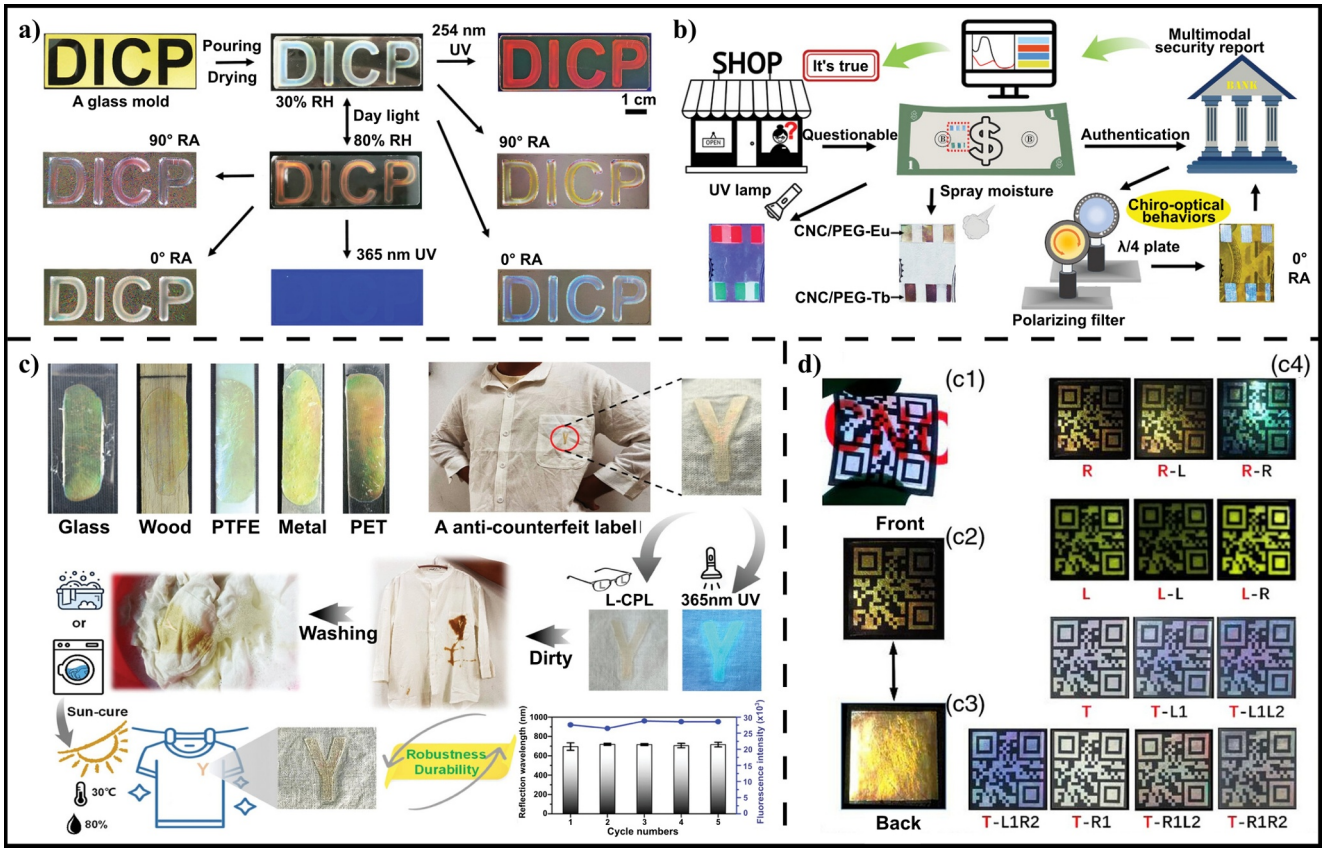

FIGURE 17 Chiral optical films for anti-counterfeiting applications. (a) Schematic illustration of the pattern printing process. (b) Schematic diagram of CNC-derived photonic composite labels on a banknote for security and anticounterfeiting. Reproduced with permission.[141a] Copyright 2022, John Wiley and Sons. (c) Application as an anticounterfeiting label. Reproduced with permission.[147] Copyright 2024, John Wiley and Sons. (d) Photographs showing laminated films of a QR code. Reproduced with permission.[144] CNC, cellulose nanocrystal; QR, quick-response.

6.3 | Displays

Wen et al.[125] introduced a versatile strategy for multicolor separation in CPCC. The CPCC was synthesized by combining a high-concentration self-assembled HPC with a cross-linked poly(acrylic acid-acrylamide) (P(AA-AM)) network. Figure 18 illustrates the applications of CPCC in display and information encryption. First, thermochromic patterned displays are showcased, featuring two unique patterns: one with a low cross-linking degree at the four corners and a high cross-linking degree at the center (Figure 18a), and the other with a low cross-linking degree in the "fish body" and a high cross-linking degree in the surrounding areas. When these CPCC samples are positioned on a heating platform, their colors shift in response to increasing temperature, displaying unique color patterns at different temperatures. Figure 18a shows patterned displays that exhibit color change with temperature. An electro-thermal device consisting of 9 pixels, each measuring 0.5 cm × 0.5 cm, was designed. The device was made from CPCC with a consistent cross-linking degree, forming an electro-thermochromic device (Figure 18b). When the same voltage was applied to the four pixelated areas, they all exhibited the same color. As the voltage increases, the color shifts from blue to red over time. As voltage can be applied to each pixel, applying voltage only to the central pixel causes color display solely in that region; By applying voltages to different pixels, multiple colors can be shown. Thus, by adjusting the voltage, any color can be displayed or changed as desired.

Zhang et al.[113] presented the E-skin based on HPC, PACA, and CNTs LC hydrogel. To explore the potential applications of the multifunctional E-skin, three red E-skin patches were applied to different fingers, and their immediate reactions to various stimuli were monitored. The E-skin on the middle finger was used to monitor signal variations during repeated interactions with an ice pack (Figure 19). Meanwhile, the E-skin on the index finger measured pressure signals generated by a pair of tweezers, and the E-skin on the thumb detected tension signals resulting from thumb bending. The material colors were observed to change visibly, including those exposed to ice, touched by tweezers, and located at the thumb joints. In addition, the electrical signals show that the material's

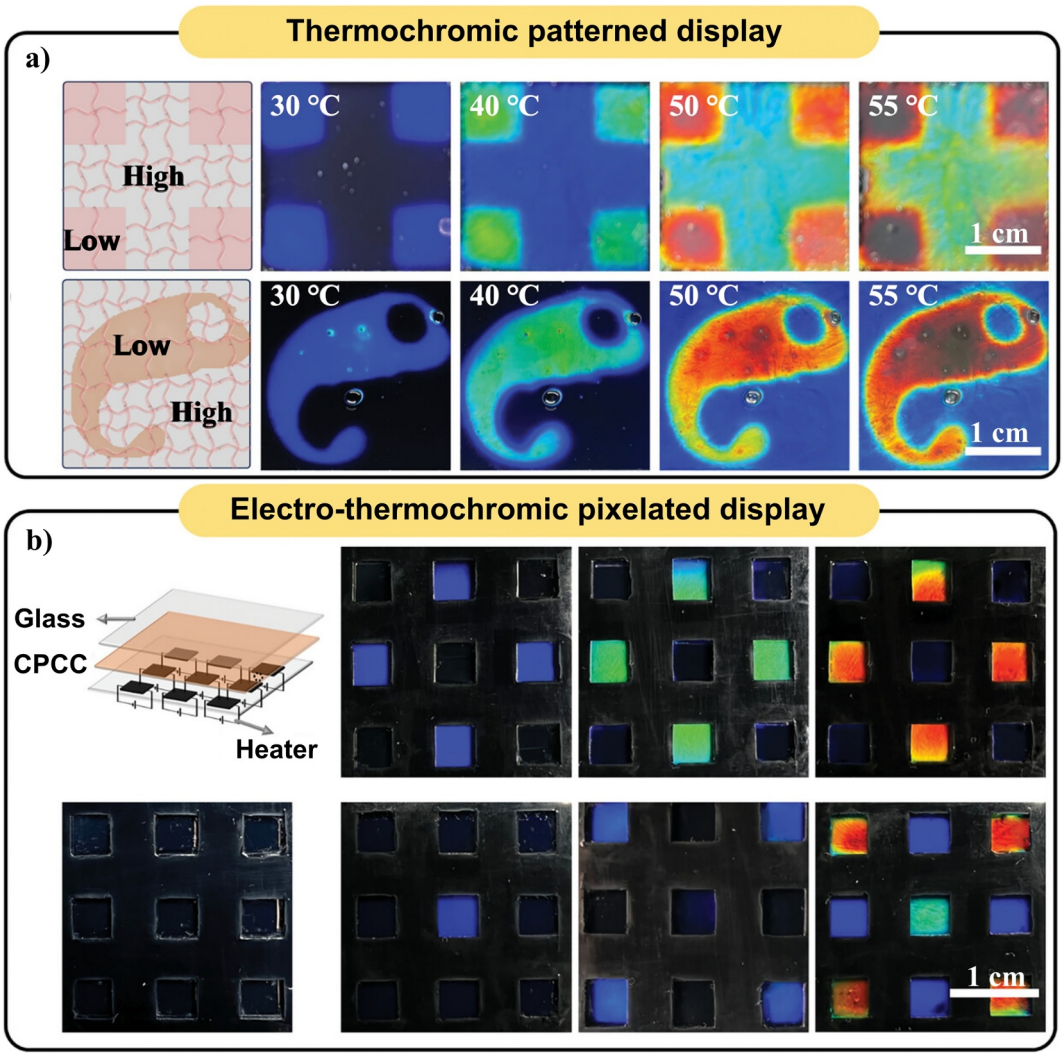

FIGURE 18 Applications for multicolor separation. (a) Thermochromic patterned display featuring low cross-linking degree at four corners and a low cross-linking degree in the "fish body." (b) Diagram and images of the pixelated electro-thermochromic device. Reproduced with permission.[125] Copyright 2024, John Wiley and Sons.

resistance varied in direct proportion to color change, allowing for easy measurement of stimuli (Figure 19b–d). Moreover, when the type of stimuli is unclear, the visual user interface acts as a guide for signal identification. A quick color shift in a particular region signals a pressure stimulus, while a gradual, directional color transition throughout the whole area indicates a tension stimulus. This signal detection capability enables visible-user interaction and resistance to interference, enhancing the multifunctional E-skin's potential for diverse applications.

6.4 | Advanced fabrics

HPC-based structurally colored fibers, known for their chirality selectivity and optical stability, provide significant advantages for the structurally colored fabrics and cutting edging materials. To showcase their potential for applications, two groups of HPC-based fibers were woven at right angles to form cohesive, stable, and flexible fabrics. By utilizing fibers with different colors and polarization states, the optical patterns and dimensions in the woven fabrics can be tailored (Figure 20a–c).[162] As proof of concept, a monochromatic fabric was produced by interweaving two sets of green fibers, yielding a flexible and foldable material (Figure 20d). A fabric featuring an HPC pattern was produced by weaving together yellow and red, green and red, and blue and red fibers. When viewed through the right-handed circular polarized filter (R-CPF) or left-handed circularly polarized filter (L-CPF), the color of the HPC-patterned fabric either becomes more pronounced or is concealed, depending on the selective

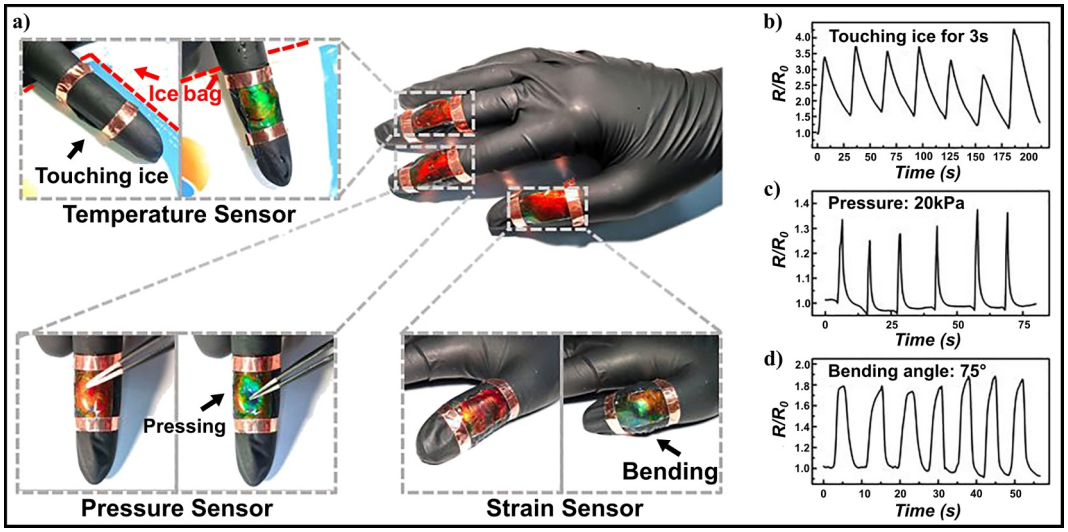

FIGURE 19 Application of multifunctional E-skins attached to human fingers based on HPC, poly(acrylamide-co-acrylic acid), and carbon nanotubes LC hydrogel. (a) Diagrams and optical images showing E-skins positioned on human fingers. Three red E-skins are attached to different fingers to monitor temperature, pressure, and strain, respectively. (b–d) Real-time resistance variations in E-skin during repeated (b) ice contact for 3 s, (c) pressure from tweezer with a pressure of 20 kPa, and (d) thumb bending angle at 75°. Reproduced with permission.[113] HPC, hydroxypropyl cellulose; LC, liquid crystal.

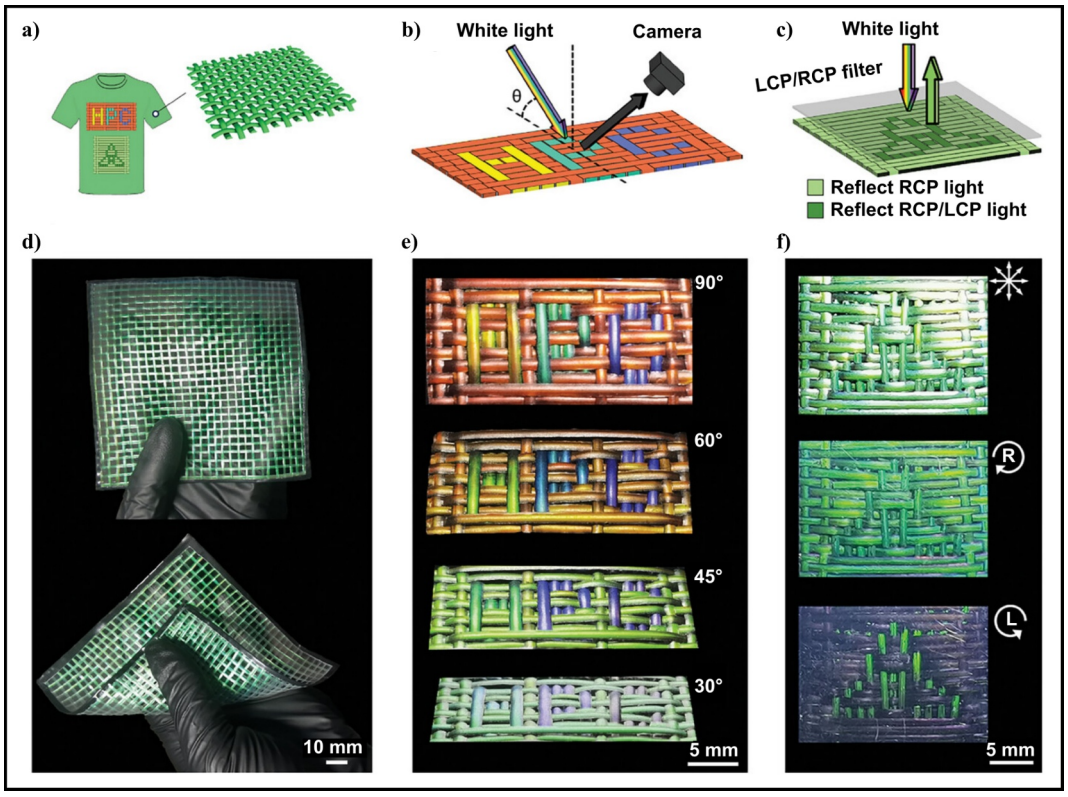

FIGURE 20 HPC-based structurally colored fibers designed for advanced performance fabrics. (a–c) HPC-based high-performance fabrics featuring color-and polarization-coded optical patterns (a), angle-dependent colors (b), and polarization-coded optical patterns (c). (d) Images of a woven fabric using single-colored fibers. (e) Images of an HPC-patterned fabric observed from various angles. (f) Images of a fabric with a trinity pattern observed under normal light, R-CPF, and L-CPF, respectively. Reproduced with permission.[162] Copyright 2024, John Wiley and Sons. HPC, hydroxypropyl cellulose; L-CPF, left-handed circularly polarized filter; R-CPF, right-handed circular polarized filter.

reflection of RCP light. The dark green fiber, which reflects both LCP and RCP light, forms the trinity flower design, whereas the light green fiber, reflecting only RCP light, constitutes the background. The fabric with the trinity pattern displays various visual effects based on the viewing conditions. When observed under white light, the fabric displays a dark trinity pattern against a light green background. However, through an R-CPF, the trinity pattern's color appears faded due to the diminished transmission of LCP light. When viewing through the L-CPF, it shows a green trinity pattern set against a dark background. These characteristics render the trinity-patterned fabric a polarization-encoded design, enabling accurate interpretation.

7 | SUMMARY AND PERSPECTIVES

Cellulose serves as the structural framework of plants, and this polymer is essential to numerous daily human activities. Materials such as wood and cellulose microfibers, which form the basis of furniture and paper, are among the most widely used cellulose-derived substances. CNCs, as one-dimensional, rod-shaped nanomaterials, are derived from naturally occurring cellulose, which is both renewable and biodegradable. CNCs are highly appealing materials due to their non-toxic nature, nanoscale size, large surface area, biodegradability, low thermal expansion, and excellent mechanical strength. The preparation of CNCs is largely dependent on their source, extraction method, conditions, yield, and crystallinity. Generally, the production of CNCs is achieved by using strong acid hydrolysis, which requires precise control of acid concentration and types, temperature, acid-to-cellulose ratio, and reaction time, resulting in distinct surface functional groups and thermal stability.

This review offers a comprehensive overview of the latest progress in the design of multi-responsive cellulose-based materials, covering the recent advances in the preparation, the structural color regulation, the manipulation of photonic properties of cellulose-based films, and potential applications. Specifically, stimuli-responsiveness includes temperature-responsiveness, humidity-responsiveness, pressure-responsiveness, tension-responsiveness, electricity-responsiveness, and magnetic force-responsiveness, and optical properties of cellulose-based composites containing circularly polarized light modulation and CPP properties are demonstrated. Subsequently, we emphasize the practical applications of these responsive materials in gas sensing, anticounterfeiting, display technologies, multifunctional E-skins, and advanced textiles, highlighting great potential for the development of next-generation cellulose-based composites in encryption and displays. Lastly, the critical challenges in existing methods and processes of CNC-based composites were highlighted, and potential solutions were proposed, integrating insights from the latest research findings. This review will foster the growth and progress of CNC-based materials. Although significant strides have been made in the fields of CNC-based composites and multiple innovative methods have been introduced to expedite the evolution of this promising area, the CNC-based composites remain in the early stages of development, and current research continues to face several obstacles.

(1) CNCs function as materials that can generate scalable chiral photonic films with superior optical properties. However, the preparation for CNCs extraction is time-consuming and the existing methods for CNCs extraction remain expensive and environmentally unfriendly. To meet the need for functional materials with tailored properties, the quest for optimal performance must be balanced with the sustainability of raw materials and their production methods. Further progress is necessary to incorporate cost-efficient and eco-friendly chemicals into the CNCs extraction process, which would greatly enhance environmental sustainability. CNC-based materials demonstrate advanced properties that surpass current cutting-edge standards. However, ongoing innovations and scientific advancements in this field will drive the development of the next generation of optically responsive materials.
(2) The understanding of CNC-based materials opens up numerous research opportunities. With global efforts in the research and development of CNC-based materials, their potential in the different fields will be explored more comprehensively. First, cellulose-based photonic structures with chiral symmetry in luminescent materials offer potential applications in chiral sensing, chiral medical imaging, enantiomer synthesis, multimodal security labels, wearable chiroptical devices, and polarization-tailored patterns. The chiro-optical systems are expected to promote the development of innovative chiral materials based on chiral cellulose templates, which could have wide-ranging applications in optical communication, information encryption, chiral sensing, advanced visual textiles, wearable chiroptical devices, smart soft robots, chemistry, and medicine. Second, CNC-based film sensors serve as affordable, disposable, and eco-friendly aldehyde detection systems with the ability for on-site monitoring. These CNC-based materials can enhance the use of biophotonics in areas such as optical anti-counterfeiting devices, information encryption, intelligent information interaction, temperature monitor, smart digital displays, and intelligent traffic recognition/control systems. Third, by leveraging the benefits of CNCs, including their availability, low cost, and biocompatibility, the CNC color manifestation approach on solid surfaces will hold great potential for the development of cost-

effective and rapid colorimetric sensors to detect volatile organic compounds and toxic gases in the near future.

(3) HPC can be utilized to develop films, microspheres, and 3D objects, showing great promise for applications in optical sensors, chiroptical filters, 3D printing, photonic pigments, anti-counterfeit coatings, and advanced fabrics. The mechanochromic behaviors, along with the capability for large-scale manufacturing, widespread commercial application, and approval for human consumption, present HPC with significant promise for biocompatible and affordable sensing applications. Furthermore, the ability to construct HPC-gels in a scalable manner using only water and food-safe ingredients will open up numerous possible applications, including mechanochromic materials with tunable responses, colorant-free food decorations, and temporary sensors in eco-friendly "smart labels" for food packaging. In addition, HPC nanoimprinted crystals provide an efficient method for generating color for packaging systems and photonic papers, with the potential to act as washable and edible detectors or labels in the food industry.

(4) The integration of CNCs with other materials can greatly expand their functionalities, and the development of advanced technologies brings new opportunities for fine processing. CNCs can serve as chiral templates to guide the arrangement of functional nanomaterials. CNC-decorated nanoparticles (CNC-NPs), especially multifunctional nanoparticles like silver, plasmonic gold nanorods, iron-oxide, palladium, and quantum dots, can be used to manipulate light polarization in chiral photonic structures. These hybrid nanocomposites take advantage of two promising materials, broadening their potential for diverse applications, including chiral lasing, energy, biomedical, biosensing, and catalysis, optical gauges and the development of multiresponsive displays and sensors. In addition, biobased and biodegradable CNC-based films like chiral CNC combined with RTP-active lignosulfonates (Lig⊂CNC films), demonstrate multicolored CPL emission, mechanical flexibility, and durability. These features make them highly promising for practical applications, including information processing, chiral polarizers, anticounterfeiting practicability, photoinduced asymmetric polymerization, visual sensing, and stereoscopic displays. The distinct features of light-emitting bio-adhesives, featuring universal adhesion and switched CPL, make them suitable for applications in optical security coding, bio-optical memory, hidden communication, and biochemical sensing. They can be used as wearable stickers, tattoos or prints, which directly attach to clothing, devices, and skin through adhesive materials that emit tailored photoluminescence. Luminescent shape-memory polymer based on CNCs with stimuli-responsive CPL are anticipated to be applied in smart skins of robotics and chiroptical switches. Furthermore, CNCs can also be used to assemble photonic membranes with a periodic chiral helical structure, making them attractive for applications like humidity sensors, camouflage materials, and smart windows. In addition, potential applications encompass optically variable films and ink pigments for security papers,[163] as well as cholesteric CNC inks for 3D structural coloration (e.g., the mixture of HPC, gelatin, and poly(acrylamide-coacrylic acid), which represent a leap forward in next-generation 3D printing. Last, the CNFs are fascinating cellulose-derived materials that provide substantial reinforcement to polymer composites, effectively improving mechanical properties while preserving structural color. All these CNC-based composite structures are particularly attractive for materials development in this field, which pushes CNC-based materials a step toward a wide range of real-world applications.

ACKNOWLEDGMENTS

The work was supported by the National Key R&D Program of China (No. 2022YFA1405000 and 2022YFA1204404), the National Natural Science Foundation of China (No. 62375141), the Natural Science Foundation of Jiangsu Province, Major Project (No. BK20243067), the National Natural Science Foundation of China (No. 62405142), the Natural Science Foundation of Jiangsu Province (No. BK20240656), Natural Science Research Start-up Foundation of Recruiting Talents of Nanjing University of Posts and Telecommunications (No. NY222053), China Postdoctoral Science Foundation (No. 2024M761391), Jiangsu Innovation Team Program, and the Fundamental Research Fund for the Central Universities.

CONFLICT OF INTEREST STATEMENT

The authors declare no conflicts of interest.

ORCID

Ye-Ming Qing https://orcid.org/0000-0002-5472-8836
Yun Ma https://orcid.org/0000-0001-8352-3760
Bing-Xiang Li https://orcid.org/0000-0003-4727-1572
Quan Li https://orcid.org/0000-0002-9042-360X

REFERENCES

1. C. He, Z. Feng, S. Shan, M. Wang, X. Chen, G. Zou, *Nat. Commun.* **2020**, *11*, 1188.
2. a) M. Cei, A. Operamolla, F. Zinna, *Adv. Opt. Mater.* **2024**, *12*, 2401714; b) J. Song, M. Wang, X. Xu, L. Qu, X. Zhou, H. Xiang, *Dalton Trans.* **2019**, *48*, 4420; c) L. Wang, A. Hao, P. Xing, *ACS Appl. Mater. Interfaces* **2022**, *14*, 44902; d) Y. Wu, M. Li, Z. G. Zheng, Z. Q. Yu, W. H. Zhu, *J. Am. Chem. Soc.* **2023**, *145*, 12951.
3. K. E. Shopsowitz, H. Qi, W. Y. Hamad, M. J. MacLachlan, *Nature* **2010**, *468*, 422.
4. a) D. Klemm, F. Kramer, S. Moritz, T. Lindström, M. Ankerfors, D. Gray, A. Dorris, *Angew. Chem. Int. Ed.* **2011**, *50*, 5438; b) J. P. F. Lagerwall, C. Schütz, M. Salajkova, J. Noh, J. Hyun Park, G. Scalia,

L. Bergström, *NPG Asia Mater.* **2014**, *6*, e80; c) S. Jia, B. Yang, J. Du, J. Zhang, Y. Xie, L. Yu, Y. Zhang, T. Tao, W. Tang, J. Gong, *Small Methods* **2024**, *8*, 2400447; d) W. Wu, Y. Xu, X. Ma, Z. Tian, C. Zhang, J. Han, X. Han, S. He, G. Duan, Y. Li, *Adv. Funct. Mater.* **2023**, *33*, 2302351; e) P. Zugenmaier, *Prog. Polym. Sci.* **2001**, *26*, 1341.

5. a) R. M. Parker, G. Guidetti, C. A. Williams, T. Zhao, A. Narkevicius, S. Vignolini, B. Frka-Petesic, *Adv. Mater.* **2017**, *30*, 1704477; b) I. A. Sacui, R. C. Nieuwendaal, D. J. Burnett, S. J. Stranick, M. Jorfi, C. Weder, E. J. Foster, R. T. Olsson, J. W. Gilman, *ACS Appl. Mater. Interfaces* **2014**, *6*, 6127; c) R. M. Brown, *J. Macromol. Sci. A.* **2006**, *33*, 1345; d) R. Zuluaga, J. L. Putaux, A. Restrepo, I. Mondragon, P. Gañán, *Cellulose* **2007**, *14*, 585; e) J. B. Gilberto Siqueira, A. Dufresne, *Biomacromolecules* **2009**, *10*, 425; f) Y. H. a. A. Dufresne, *Biomacromolecules* **2008**, *9*, 1974; g) Y. N. Tsuguyuki Saito, J. L. Putaux, M. Vignon, A. Isogai, *Biomacromolecules* **2006**, *7*, 6; h) A. Alemdar, M. Sain, *Bioresour. Technol.* **2008**, *99*, 1664; i) B. Wang, M. Sain, *Compos. Sci. Technol.* **2007**, *67*, 2521; j) T. Imai, J. Sugiyama, *Macromolecules* **1998**, *31*, 6275; k) X. D. Cao, H. Dong, C. M. Li, *Biomacromolecules* **2007**, *8*, 899; l) T. Zimmermann, N. Bordeanu, E. Strub, *Carbohydr. Polym.* **2010**, *79*, 1086; m) S. Elazzouzi-Hafraoui, Y. Nishiyama, J. L. Putaux, L. Heux, F. Dubreuil, C. Rochas, *Biomacromolecules* **2008**, *9*, 57; n) J. Leitner, B. Hinterstoisser, M. Wastyn, J. Keckes, W. Gindl, *Cellulose* **2007**, *14*, 419.
6. a) Y. Nishio, in *Polysaccharides II*, Vol. 205 (Ed: D. Klemm), Springer, Berlin, Heidelberg **2006**, p. 97; b) R. S. J. M. Yoshiyuki Nishio, R. S. J. Manley, *Macromolecules* **1988**, *21*, 1270.
7. a) A. W. Baochun Wang, A. Walther, *ACS Nano* **2015**, *9*, 10637; b) A. Tran, C. E. Boott, M. J. MacLachlan, *Adv. Mater.* **2020**, *32*, 1905876.
8. Y. Chen, L. Zhang, Y. Yang, B. Pang, W. Xu, G. Duan, S. Jiang, K. Zhang, *Adv. Mater.* **2021**, *33*, 2005569.
9. R. J. Moon, A. Martini, J. Nairn, J. Simonsen, J. Youngblood, *Chem. Soc. Rev.* **2011**, *40*, 3941.
10. D. Trache, A. F. Tarchoun, M. Derradji, T. S. Hamidon, N. Masruchin, N. Brosse, M. H. Hussin, *Front. Chem.* **2020**, *8*, 392.
11. a) A. G. Dumanli, G. Kamita, J. Landman, H. van der Kooij, B. J. Glover, J. J. Baumberg, U. Steiner, S. Vignolini, *Adv. Opt. Mater.* **2014**, *2*, 646; b) S. N. Fernandes, P. L. Almeida, N. Monge, L. E. Aguirre, D. Reis, C. L. P. de Oliveira, A. M. F. Neto, P. Pieranski, M. H. Godinho, *Adv. Mater.* **2016**, *29*, 1603560.
12. H. Águas, T. Mateus, A. Vicente, D. Gaspar, M. J. Mendes, W. A. Schmidt, L. Pereira, E. Fortunato, R. Martins, *Adv. Funct. Mater.* **2015**, *25*, 3592.
13. D. Ha, Z. Fang, L. Hu, J. N. Munday, *Adv. Energy Mater.* **2014**, *4*, 1301804.
14. A. Espinha, G. Guidetti, M. C. Serrano, B. Frka-Petesic, A. G. Dumanli, W. Y. Hamad, Á. Blanco, C. López, S. Vignolini, *ACS Appl. Mater. Interfaces* **2016**, *8*, 31935.
15. T. Wu, J. Li, J. Li, S. Ye, J. Wei, J. Guo, *J. Mater. Chem. C* **2016**, *4*, 9687.
16. L. Polavarapu, L. M. Liz-Marzan, *Phys. Chem. Chem. Phys.* **2013**, *15*, 5288.
17. A. Espinha, C. Dore, C. Matricardi, M. I. Alonso, A. R. Goñi, A. Mihi, *Nat. Photonics* **2018**, *12*, 343.
18. a) C. C. Wan, Y. Jiao, W. Y. Tian, L. Y. Zhang, Y. Q. Wu, J. Li, X. J. Li, *Chem. Eng. J.* **2020**, *393*, 124637; b) J. Han, K. Lu, Y. Yue, C. Mei, C. Huang, Q. Wu, X. Xu, *Ind. Crops Prod.* **2019**, *128*, 94.
19. a) X. Wang, M. Li, Y. Xiong, H. Qin, Q. Li, F. Zhang, Y. L. Yu, G. Qing, *Small* **2024**, *21*, e2408695; b) S. Wang, X. Dai, D. Fu, F. Wang, L. Zhang, J. Shen, *Cellulose* **2024**, *31*, 6211.
20. H. Golmohammadi, E. Morales-Narváez, T. Naghdi, A. Merkoçi, *Chem. Mater.* **2017**, *29*, 5426.
21. M. E. G. Rui, M. A. Domingues, R. L. Reis, *Biomacromolecules* **2014**, *15*, 2327.
22. G. Mondragon, A. Santamaria-Echart, M. E. V. Hormaiztegui, A. Arbelaiz, C. Peña-Rodriguez, V. Mucci, M. Corcuera, M. I. Aranguren, A. Eceiza, *J. Polym. Environ.* **2017**, *26*, 1869.
23. a) T. Hiratani, W. Y. Hamad, M. J. MacLachlan, *Adv. Mater.* **2017**, *29*, 1606083; b) G. Guidetti, S. Atifi, S. Vignolini, W. Y. Hamad, *Adv. Mater.* **2016**, *28*, 10042.
24. G. Chu, X. Wang, H. Yin, Y. Shi, H. Jiang, T. Chen, J. Gao, D. Qu, Y. Xu, D. Ding, *ACS Appl. Mater. Interfaces* **2015**, *7*, 21797.
25. a) Z. Huang, V. S. Raghuwanshi, G. Garnier, *Front. Bioeng. Biotechnol.* **2017**, *5*, 41; b) V. S. Raghuwanshi, J. Su, C. J. Garvey, S. A. Holt, W. Raverty, R. F. Tabor, P. J. Holden, M. Gillon, W. Batchelor, G. Garnier, *Cellulose* **2016**, *24*, 11.
26. L. Hossain, V. S. Raghuwanshi, J. Tanner, G. Garnier, *Colloids Surf.* **2021**, *630*, 127608.
27. Q. F. Guan, H. B. Yang, Z. M. Han, L. C. Zhou, Y. B. Zhu, Z. C. Ling, H. B. Jiang, P. F. Wang, T. Ma, H. A. Wu, S. H. Yu, *Sci. Adv.* **2020**, *6*, eaaz1114.
28. a) D. Zhang, H. Zheng, X. Ma, L. Su, X. Gao, Z. Tang, Y. Xu, *Adv. Opt. Mater.* **2022**, *10*, 2102015; b) K. Adstedt, E. A. Popenov, K. J. Pierce, R. Xiong, R. Geryak, V. Cherpak, D. Nepal, T. J. Bunning, V. V. Tsukruk, *Adv. Funct. Mater.* **2020**, *30*, 2003597; c) B. Dimitrov, D. Bukharina, V. Poliukhova, D. Nepal, M. E. McConney, T. J. Bunning, V. V. Tsukruk, *ACS Appl. Opt. Mater.* **2024**, *2*, 2540; d) D. Gray, *Nanomaterials* **2016**, *6*, 213.
29. H. B. Revol, J. Giasson, R. H. Marchessault, D. G. Gray, *Int. J. Biol. Macromol.* **1992**, *14*, 170.
30. a) D. Qu, M. Archimi, A. Camposeo, D. Pisignano, E. Zussman, *ACS Nano* **2021**, *15*, 8753; b) M. Xu, X. Wu, Y. Yang, C. Ma, W. Li, H. Yu, Z. Chen, J. Li, K. Zhang, S. Liu, *ACS Nano* **2020**, *14*, 11130.
31. a) O. Kose, A. Tran, L. Lewis, W. Y. Hamad, M. J. MacLachlan, *Nat. Commun.* **2019**, *10*, 510; b) M. Mitov, *Soft Matter* **2017**, *13*, 4176; c) Q. Chen, P. Liu, F. Nan, L. Zhou, J. Zhang, *Biomacromolecules* **2014**, *15*, 4343; d) F. Jativa, C. Schütz, L. Bergström, X. Zhang, B. Wicklein, *Soft Matter* **2015**, *11*, 5374.
32. a) S. Jia, B. Yang, Y. Xie, T. Tao, J. Du, L. Yu, Y. Zhang, J. Zhang, W. Tang, J. Gong, *Adv. Funct. Mater.* **2024**, *36*, 7967; b) X. Mu, D. G. Gray, *Cellulose* **2015**, *22*, 1103.
33. C. H. Barty-King, C. L. C. Chan, R. M. Parker, M. M. Bay, R. Vadrucci, M. De Volder, S. Vignolini, *Adv. Mater.* **2021**, *33*, e2102112.
34. R. S. Werbowyj, D. G. Gray, *Mol. Cryst. Liq. Cryst.* **2007**, *34*, 97.
35. Z. L. Zhang, X. Dong, Y. Y. Zhao, F. Song, X. L. Wang, Y. Z. Wang, *Biomacromolecules* **2022**, *23*, 4110.
36. a) V. Sharma, M. Crne, J. O. Park, M. Srinivasarao, *Science* **2009**, *325*, 449; b) K. Yao, Q. Meng, V. Bulone, Q. Zhou, *Adv. Mater.* **2017**, *29*, 1701323.
37. T. Chiou, S. Kleinlogel, T. Cronin, R. Caldwell, B. Loeffler, A. Siddiqi, A. Goldizen, J. Marshall, *Curr. Biol.* **2008**, *18*, 429.
38. a) M. Xu, C. Ma, J. Zhou, Y. Liu, X. Wu, S. Luo, W. Li, H. Yu, Y. Wang, Z. Chen, J. Li, S. Liu, *J. Mater. Chem. C* **2019**, *7*, 13794; b) S. Hirata, M. Vacha, *J. Phys. Chem. Lett.* **2016**, *7*, 1539; c) W. Chen, Z. Tian, Y. Li, Y. Jiang, M. Liu, P. Duan, *Chem. - Eur. J.* **2018**, *24*, 17444; d) H. Li, H. Li, W. Wang, Y. Tao, S. Wang, Q. Yang, Y. Jiang, C. Zheng, W. Huang, R. Chen, *Angew. Chem. Int. Ed.* **2020**, *59*, 4756; e) H. Li, J. Gu, Z. Wang, J. Wang, F. He, P. Li, Y. Tao, H. Li, G. Xie, W. Huang, C. Zheng, R. Chen, *Nat. Commun.* **2022**, *13*, 429; f) S. Garain, S. Sarkar, B. Chandra Garain, S. K. Pati, S. J. George, *Angew. Chem. Int. Ed.* **2022**, *61*, e202115773; g) W. Hao, Y. Li, M. Liu, *Adv. Opt. Mater.* **2021**, *9*, 2100452; h) Z. Geng, Y. Zhang, Y. Zhang, Y. Li, Y. Quan, Y. Cheng, *J. Mater. Chem. C* **2021**, *9*, 12141; i) B. Yue, X. Feng, C. Wang, M. Zhang, H. Lin, X. Jia, L. Zhu, *ACS Nano* **2022**, *16*, 16201; j) R. Inoue, R. Kondo, Y. Morisaki, *Chem. Mater.* **2022**, *34*, 7959; k) T. R. Schulte, J. J. Holstein, L. Krause, R. Michel, D. Stalke, E. Sakuda, K. Umakoshi, G. Longhi, S. Abbate, G. H. Clever, *J. Am. Chem. Soc.* **2017**, *139*, 6863; l) T. Usuki, H. Uchida, K. Omoto, Y. Yamanoi, A. Yamada, M. Iwamura, K. Nozaki,

H. Nishihara, *J. Org. Chem.* **2019**, *84*, 10749; m) G. Park, H. Kim, H. Yang, K. R. Park, I. Song, J. H. Oh, C. Kim, Y. You, *Chem. Sci.* **2019**, *10*, 1294; n) J. M. Heo, J. Kim, M. I. Hasan, H. Woo, J. Lahann, J. Kim, *Adv. Opt. Mater.* **2024**, *12*, 2400572; o) D. Y. Liu, H. Y. Li, R. P. Han, H. L. Liu, S. Q. Zang, *Angew. Chem. Int. Ed.* **2023**, *62*, e202307875; p) S. Li, Y. Tang, Q. Fan, Z. Li, X. Zhang, J. Wang, J. Guo, Q. Li, *Light Sci. Appl.* **2024**, *13*, 140.

39. a) J. Han, S. Guo, J. Wang, L. Wei, Y. Zhuang, S. Liu, Q. Zhao, X. Zhang, W. Huang, *Adv. Opt. Mater.* **2017**, *5*, 1700359; b) G. Lu, Z. G. Wu, R. Wu, X. Cao, L. Zhou, Y.-X. Zheng, C. Yang, *Adv. Funct. Mater.* **2021**, *31*, 2102898.
40. T. Li, C. Chen, A. H. Brozena, J. Y. Zhu, L. Xu, C. Driemeier, J. Dai, O. J. Rojas, A. Isogai, L. Wågberg, L. Hu, *Nature* **2021**, *590*, 47.
41. V. S. Raghuwanshi, G. Garnier, *Adv. Funct. Mater.* **2024**, *35*, 2412869.
42. X. Lin, D. Shi, G. Yi, D. Yu, *Responsive Mater.* **2024**, *2*, e20230031.
43. a) Y. Yang, X. Zhang, C. Valenzuela, R. Bi, Y. Chen, Y. Liu, C. Zhang, W. Li, L. Wang, W. Feng, *Matter* **2024**, *7*, 2091; b) W. Yang, S. Xiao, Q. Song, Y. Liu, Y. Wu, S. Wang, J. Yu, J. Han, D. Tsai, *Nat. Commun.* **2020**, *11*, 1864.
44. a) S. Vignolini, P. J. Rudall, A. V. Rowland, A. Reed, E. Moyroud, R. B. Faden, J. J. Baumberg, B. J. Glover, U. Steiner, *Proc. Natl. Acad. Sci. U. S. A.* **2012**, *109*, 15712; b) V. Pete, *Science* **2009**, *325*, 398.
45. a) X. Zhang, Y. Yang, P. Xue, C. Valenzuela, Y. Chen, X. Yang, L. Wang, W. Feng, *Angew. Chem. Int. Ed.* **2022**, *61*, 2211030; b) W. Lu, M. Si, X. Le, T. Chen, *Acc. Chem. Res.* **2022**, *55*, 2291.
46. N. C. Grassly, C. Fraser, G. P. Garnett, *Nature* **2005**, *433*, 417.
47. S. Poppinga, C. Zollfrank, O. Prucker, J. Ruhe, A. Menges, T. Cheng, T. Speck, *Adv. Mater.* **2018**, *30*, e1703653.
48. J. Teyssier, S. V. Saenko, D. van der Marel, M. C. Milinkovitch, *Nat. Commun.* **2015**, *6*, 6368.
49. Y. Wang, H. Cui, Q. Zhao, X. Du, *Matter* **2019**, *1*, 626.
50. a) A. R. Parker, H. E. Townley, *Nat. Nanotechnol.* **2007**, *2*, 347; b) J. Jeon, D. Bukharina, M. Kim, S. Kang, J. Kim, Y. Zhang, V. Tsukruk, *Responsive Mater.* **2024**, *2*, e20230032.
51. J. C. Weaver, G. W. Milliron, A. Miserez, K. Evans-Lutterodt, S. Herrera, I. Gallana, W. J. Mershon, B. Swanson, P. Zavattieri, E. DiMasi, D. Kisailus, *Science* **2012**, *336*, 1275.
52. H. K. Bisoyi, Q. Li, *Chem. Rev.* **2022**, *122*, 4887.
53. S. Kinoshita, S. Yoshioka, J. Miyazaki, *Rep. Prog. Phys.* **2008**, *71*, 076401.
54. W. J. Choi, G. Cheng, Z. Huang, S. Zhang, T. B. Norris, N. A. Kotov, *Nat. Mater.* **2019**, *18*, 820.
55. E. Tian, J. Wang, Y. Zheng, Y. Song, L. Jiang, D. Zhu, *J. Mater. Chem.* **2008**, *18*, 1116.
56. Y. Ohtsuka, T. Seki, Y. Takeoka, *Angew. Chem. Int. Ed.* **2015**, *54*, 15368.
57. E. Tian, Y. Ma, L. Cui, J. Wang, Y. Song, L. Jiang, *Macromol. Rapid Commun.* **2009**, *30*, 1719.
58. K. Ueno, J. Sakamoto, Y. Takeoka, M. Watanabe, *J. Mater. Chem.* **2009**, *19*, 4778.
59. C. I. Aguirre, E. Reguera, A. Stein, *Adv. Funct. Mater.* **2010**, *20*, 2565.
60. a) L. A. L. Youssef Habibi, O. J. Rojas, *Chem. Rev.* **2010**, *110*, 3479; b) S. Eyley, S. Shariki, S. E. C. Dale, S. Bending, F. Marken, W. Thielemans, *Langmuir* **2012**, *28*, 6514.
61. F. Cherhal, F. Cousin, I. Capron, *Langmuir* **2015**, *31*, 5596.
62. H. Liu, J. Song, S. Shang, Z. Song, D. Wang, *ACS Appl. Mater. Interfaces* **2012**, *4*, 2413.
63. O. M. Vanderfleet, E. D. Cranston, *Nat. Rev. Mater.* **2020**, *6*, 124.
64. L. Chen, Q. Wang, K. Hirth, C. Baez, U. P. Agarwal, J. Y. Zhu, *Cellulose* **2015**, *22*, 1753.
65. R. Leiner, S. Witayakran, S. Verwaayen, L. Siegwardt, C. C. Ribeiro, C. Dietz, M. Koch, A. Kulachenko, M. Gallei, *ACS Appl. Mater. Interfaces* **2024**, *16*, 64377.
66. Y. Tang, H. Yang, S. Vignolini, *Adv. Sustainable Syst.* **2022**, *6*, 2100100.
67. E. J. Foster, R. J. Moon, U. P. Agarwal, M. J. Bortner, J. Bras, S. Camarero-Espinosa, K. J. Chan, M. J. D. Clift, E. D. Cranston, S. J. Eichhorn, D. M. Fox, W. Y. Hamad, L. Heux, B. Jean, M. Korey, W. Nieh, K. J. Ong, M. S. Reid, S. Renneckar, R. Roberts, J. A. Shatkin, J. Simonsen, K. Stinson-Bagby, N. Wanasekara, J. Youngblood, *Chem. Soc. Rev.* **2018**, *47*, 2609.
68. a) E. Kontturi, A. Meriluoto, P. A. Penttilä, N. Baccile, J. M. Malho, A. Potthast, T. Rosenau, J. Ruokolainen, R. Serimaa, J. Laine, H. Sixta, *Angew. Chem. Int. Ed.* **2016**, *55*, 14455; b) M. Lorenz, S. Sattler, M. Reza, A. Bismarck, E. Kontturi, *Faraday Discuss.* **2017**, *202*, 315.
69. a) J. Guo, I. Filpponen, L. S. Johansson, P. Mohammadi, M. Latikka, M. B. Linder, R. H. A. Ras, O. J. Rojas, *Biomacromolecules* **2017**, *18*, 898; b) N. S. Semenikhin, N. R. Kadasala, R. J. Moon, J. W. Perry, K. H. Sandhage, *Langmuir* **2018**, *34*, 4427.
70. M. Cheng, Z. Qin, Y. Chen, S. Hu, Z. Ren, M. Zhu, *ACS Sustainable Chem. Eng.* **2017**, *5*, 4656.
71. a) R. F. L. Kusmono, M. W. Wildan, M. N. Ilman, *Heliyon* **2020**, *6*, e05486; b) Z. Pang, P. Wang, C. Dong, *Cellulose* **2018**, *25*, 7053; c) V. F. Korolovych, V. Cherpak, D. Nepal, A. Ng, N. R. Shaikh, A. Grant, R. Xiong, T. J. Bunning, V. V. Tsukruk, *Polymer* **2018**, *145*, 334; d) K. N. M. Amin, A. Hosseinmardi, D. J. Martin, P. K. Annamalai, *J. Bioresour. Bioprod.* **2022**, *7*, 99.
72. a) M. A. Smirnov, M. P. Sokolova, D. A. Tolmachev, V. K. Vorobiov, I. A. Kasatkin, N. N. Smirnov, A. V. Klaving, N. V. Bobrova, N. V. Lukasheva, A. V. Yakimansky, *Cellulose* **2020**, *27*, 4305; b) X. Li, C. Ning, L. Li, W. Liu, Q. Ren, Q. Hou, *Carbohydr. Polym.* **2021**, *274*, 118650; c) S. Liu, Z. Tian, X. X. Ji, M. G. Ma, *Cellulose* **2024**, *31*, 2175.
73. X. Yang, H. Xie, H. Du, X. Zhang, Z. Zou, Y. Zou, W. Liu, H. Lan, X. Zhang, C. Si, *ACS Sustainable Chem. Eng.* **2019**, *7*, 7200.
74. a) L. Wang, A. M. Urbas, Q. Li, X. Dou, *Adv. Mater.* **2020**, *32*, e1801335; b) R. Lan, X. G. Hu, J. Chen, X. Zeng, X. Chen, T. Du, X. Song, H. Yang, *Responsive. Mater.* **2024**, *2*, e20230030.
75. Z. Zhang, X. Yang, Y. Zhao, F. Ye, L. Shang, *Adv. Mater.* **2023**, *35*, 2300220.
76. H. K. Bisoyi, Q. Li, *Chem. Rev.* **2016**, *116*, 15089.
77. J. F. Revol, L. Godbout, X. M. Dong, D. G. Gray, H. Chanzy, G. Maret, *Liq. Cryst.* **1994**, *16*, 127.
78. a) J. Li, H. K. Bisoyi, J. Tian, J. Guo, Q. Li, *Adv. Mater.* **2019**, *31*, 1807751; b) L. Wang, Q. Li, *Chem. Soc. Rev.* **2018**, *47*, 1044.
79. C. Yuan, W. Huang, Z. Zheng, B. Liu, H. Bisoyi, Y. Li, D. Shen, Y. Lu, Q. Li, *Sci. Adv.* **2019**, *5*, eaax9501.
80. a) S. Lin, H. Sun, J. Qiao, X. Ding, J. Guo, *Adv. Opt. Mater.* **2020**, *8*, 2000107; b) Z.-G. Zheng, Y. Li, H. K. Bisoyi, L. Wang, T. J. Bunning, Q. Li, *Nature* **2016**, *531*, 352.
81. a) J. Pan, W. Hamad, S. K. Straus, *Macromolecules* **2010**, *43*, 3851; b) S. Beck, J. Bouchard, G. Chauve, R. Berry, *Cellulose* **2013**, *20*, 1401.
82. a) J. B. Stephanie Beck, R. Berry, *Biomacromolecules* **2011**, *12*, 167; b) J. H. Park, J. Noh, C. Schütz, G. Salazar-Alvarez, G. Scalia, L. Bergström, J. P. F. Lagerwall, *Chem. Phys. Chem.* **2014**, *15*, 1477.
83. T. K. Fumiko Kimura, M. Tamura, A. Hirai, M. Ikuno, F. Horii, F. Horii, *Langmuir* **2005**, *21*, 2034.
84. a) D. Bordel, J. Putaux, L. Heux, *Langmuir* **2006**, *22*, 4899; b) Y. Habibi, T. Heim, R. Douillard, *J. Polym. Sci., Part B: Polym. Phys.* **2008**, *46*, 1430; c) R. Bohoslavsky, M. G. Witte, T. M. Janssen, M. van Herk, *Phys. Med. Biol.* **2013**, *58*, 3563; d) B. Frka-Petesic, H. Radavidson, B. Jean, L. Heux, *Adv. Mater.* **2017**, *29*, 1606208.
85. D. Li, J. M. Wu, Z. H. Liang, L. Y. Li, X. Dong, S. K. Chen, T. Fu, X. L. Wang, Y. Z. Wang, F. Song, *Adv. Sci.* **2022**, *10*, 2206290.
86. a) L. S. Fanfan Fu, Z. Chen, Y. Yu, Y. Zhao, Y. Zhao, *Sci. Robot.* **2018**, *3*, eaar8580; b) P. V. Brann, *Nature* **2011**, *472*, 423; c) S.

Tadepalli, J. M. Slocik, M. K. Gupta, R. R. Naik, S. Singamaneni, *Chem. Rev.* **2017**, *117*, 12705; d) I. C. Cuthill, W. L. Allen, K. Arbuckle, B. Caspers, G. Chaplin, M. E. Hauber, G. E. Hill, N. G. Jablonski, C. D. Jiggins, A. Kelber, J. Mappes, J. Marshall, R. Merrill, D. Osorio, R. Prum, N. W. Roberts, A. Roulin, H. M. Rowland, T. N. Sherratt, J. Skelhorn, M. P. Speed, M. Stevens, M. C. Stoddard, D. Stuart-Fox, L. Talas, E. Tibbetts, T. Caro, *Science* **2017**, *357*, eaan0221; e) M. M. Ito, A. H. Gibbons, D. Qin, D. Yamamoto, H. Jiang, D. Yamaguchi, K. Tanaka, E. Sivaniah, *Nature* **2019**, *570*, 363.

87. a) M. Vatankhah-Varnosfaderani, A. N. Keith, Y. Cong, H. Liang, M. Rosenthal, M. Sztucki, C. Clair, S. Magonov, D. A. Ivanov, A. V. Dobrynin, S. S. Sheiko, *Science* **2018**, *359*, 1509; b) Y. Zhao, Z. Xie, H. Gu, C. Zhu, Z. Gu, *Chem. Soc. Rev.* **2012**, *41*, 3297.
88. a) J. H. Kim, J. H. Moon, S. Lee, J. Park, *Appl. Phys. Lett.* **2010**, *97*, 202106; b) C. Xu, G. T. Stiubianu, A. A. Gorodetsky, *Science* **2018**, *359*, 1495; c) H. Kim, J. Ge, J. Kim, S. Choi, H. Lee, H. Lee, W. Park, Y. Yin, S. Kwon, *Nat. Photonics* **2009**, *3*, 534; d) J. Hou, H. Zhang, Q. Yang, M. Li, Y. Song, L. Jiang, *Angew. Chem. Int. Ed.* **2014**, *53*, 5791; e) L. Chen, B. Su, L. Jiang, *Chem. Soc. Rev.* **2019**, *48*, 8; f) J. Sun, X. Ji, G. Li, Y. Zhang, N. Liu, H. Li, M. Qin, Z. Yuan, *J. Mater. Chem. C* **2019**, *7*, 104; g) L. Liu, R. Aleisa, Y. Zhang, J. Feng, Y. Zheng, Y. Yin, W. Wang, *Angew. Chem. Int. Ed.* **2019**, *58*, 16307; h) C. Zhao, H. Li, Y. Wang, K. Li, J. Hou, Y. Ma, M. Li, Y. Song, *Adv. Opt. Mater.* **2019**, *7*, 1900127; i) M. Su, Y. Sun, B. Chen, Z. Zhang, X. Yang, S. Chen, Q. Pan, D. Zuev, P. Belov, Y. Song, *Sci. Bull.* **2021**, *66*, 250; j) M. Qin, M. Sun, M. Hua, X. He, *Curr. Opin. Solid State Mater. Sci.* **2019**, *23*, 13; k) D. P. Puzzo, A. C. Arsenault, I. Manners, G. A. Ozin, *Angew. Chem.* **2009**, *121*, 961; l) Y. Yue, T. Kurokawa, M. A. Haque, T. Nakajima, T. Nonoyama, X. Li, I. Kajiwara, J. P. Gong, *Nat. Commun.* **2014**, *5*, 4659; m) D. Ge, E. Lee, L. Yang, Y. Cho, M. Li, D. S. Gianola, S. Yang, *Adv. Mater.* **2015**, *27*, 2489; n) M. Kolle, P. M. Salgard-Cunha, M. R. J. Scherer, F. Huang, P. Vukusic, S. Mahajan, J. J. Baumberg, U. Steiner, *Nat. Nanotechnol.* **2010**, *5*, 511.
89. a) D. Guo, C. Chen, C. Li, H.-C. Jau, K. Lin, T. M. Feng, C. Wang, T. J. Bunning, I. C. Khoo, T. H. Lin, *Nat. Mater.* **2019**, *19*, 94; b) H. Lu, J. Ma, Y. Li, S. Bokhari, X. Jiang, S. Zhu, D. Zhang, *ACS Appl. Mater. Interfaces* **2017**, *9*, 18231; c) J. A. Kelly, A. M. Shukaliak, C. C. Y. Cheung, K. E. Shopsowitz, W. Y. Hamad, M. J. MacLachlan, *Angew. Chem.* **2013**, *125*, 9080; d) T. Hayata, M. Fukawa, S. Furumi, *J. Photopolym. Sci. Technol.* **2019**, *32*, 645; e) W. Zou, X. Lin, E. M. Terentjev, *Adv. Mater.* **2021**, *33*, 2101955.
90. a) Y. Li, J. Jun-Yan Suen, E. Prince, E. M. Larin, A. Klinkova, H. Thérien-Aubin, S. Zhu, B. Yang, A. S. Helmy, O. D. Lavrentovich, E. Kumacheva, *Nat. Commun.* **2016**, *7*, 12520; b) L. Qin, X. Liu, K. He, G. Yu, H. Yuan, M. Xu, F. Li, Y. Yu, *Nat. Commun.* **2021**, *12*, 699.
91. Z. Zhang, Z. Chen, Y. Wang, Y. Zhao, L. Shang, *Adv. Funct. Mater.* **2021**, *32*, 2107242.
92. Z. Zhang, C. Wang, Q. Wang, Y. Zhao, L. Shang, *Proc. Natl. Acad. Sci. U. S. A.* **2022**, *119*, e2204113119.
93. C. L. C. Chan, I. M. Lei, G. T. van de Kerkhof, R. M. Parker, K. D. Richards, R. C. Evans, Y. Y. S. Huang, S. Vignolini, *Adv. Funct. Mater.* **2022**, *32*, 2108566.
94. S. Lu, B. Du, S. A. Khan, S. Huang, *Adv. Funct. Mater.* **2024**, *34*, 2406902.
95. G. Zhao, Y. Huang, C. Mei, S. Zhai, Y. Xuan, Z. Liu, M. Pan, O. J. Rojas, *Small* **2021**, *17*, 2103936.
96. a) X. Qiu, Q. Cui, Q. Guo, T. Zhou, X. Zhang, M. Tian, *Small* **2022**, *18*, 2107164; b) A. P. C. Almeida, J. P. Canejo, S. N. Fernandes, C. Echeverria, P. L. Almeida, M. H. Godinho, *Adv. Mater.* **2018**, *30*, 1703655; c) Y. Y. Wang, X. Huang, X. X. Zhang, *Nat. Commun.* **2021**, *12*, 1291.
97. J. N. Lythgoe, J. Shand, R. G. Foster, *Nature* **1984**, *308*, 83.
98. Y. Sun, Y. Wang, Y. Liu, S. Wu, S. Zhang, W. Niu, *Adv. Funct. Mater.* **2022**, *32*, 2204467.
99. a) X. Li, J. Liu, D. Li, S. Huang, K. Huang, X. Zhang, *Adv. Sci.* **2021**, *8*, 2101295; b) M. Xu, G. Li, W. Li, B. An, J. Sun, Z. Chen, H. Yu, J. Li, G. Yang, S. Liu, *Angew. Chem. Int. Ed.* **2022**, *61*, e202117042.
100. a) P. Lv, X. Lu, L. Wang, W. Feng, *Adv. Funct. Mater.* **2021**, *31*, 2104991; b) P. R. Anusuyadevi, R. Shanker, Y. Cui, A. V. Riazanova, M. Järn, M. P. Jonsson, A. J. Svagan, *Adv. Mater.* **2021**, *33*, 2101519.
101. Y. Liu, P. Wu, S. Wu, *Adv. Funct. Mater.* **2020**, *30*, 2002193.
102. Y. Sui, X. Li, W. Chang, H. Wan, W. Li, F. Yang, Z. Z. Yu, *Carbohydr. Polym.* **2020**, *232*, 115778.
103. H. Chen, A. Hou, C. Zheng, J. Tang, K. Xie, A. Gao, *ACS Appl. Mater. Interfaces* **2020**, *12*, 24505.
104. W. Song, J. K. Lee, M. S. Gong, K. Heo, W.-J. Chung, B. Y. Lee, *ACS Appl. Mater. Interfaces* **2018**, *10*, 10353.
105. Y. Cao, L. Lewis, W. Y. Hamad, M. J. MacLachlan, *Adv. Mater.* **2019**, *31*, 1808186.
106. M. Shi, L. Bai, D. Wan, J. Chang, Q. Li, H. Yu, S. Liu, T. Wei, W. Chen, Z. Fan, *Matter* **2022**, *5*, 2813.
107. X. Li, J. Liu, X. Zhang, *Adv. Funct. Mater.* **2023**, *33*, 2306208.
108. a) J. C. Yang, J. Mun, S. Y. Kwon, S. Park, Z. Bao, S. Park, *Adv. Mater.* **2019**, *31*, 1904765; b) J. Y. Oh, Z. Bao, *Adv. Sci.* **2019**, *6*, 1900186; c) C. M. Boutry, L. Beker, Y. Kaizawa, C. Vassos, H. Tran, A. C. Hinckley, R. Pfattner, S. Niu, J. Li, J. Claverie, Z. Wang, J. Chang, P. M. Fox, Z. Bao, *Nat. Biomed. Eng.* **2019**, *3*, 47; d) D. Son, Z. Bao, *ACS Nano* **2018**, *12*, 11731.
109. a) Y. Yu, J. Guo, L. Sun, X. Zhang, Y. Zhao, *Research* **2019**, *2019*, 6906275; b) J. Xu, H.-C. Wu, C. Zhu, A. Ehrlich, L. Shaw, M. Nikolka, S. Wang, F. Molina-Lopez, X. Gu, S. Luo, D. Zhou, Y. Kim, G.-J. N. Wang, K. Gu, V. R. Feig, S. Chen, Y. Kim, T. Katsumata, Y. Zheng, H. Yan, J. W. Chung, J. Lopez, B. Murmann, Z. Bao, *Nat. Mater.* **2019**, *18*, 594; c) H. Xia, Y. Ran, H. Li, X. Tao, D. Wang, *J. Mater. Chem. A.* **2013**, *1*, 4678; d) S. R. Shin, Y. Li, H. L. Jang, P. Khoshakhlagh, M. Akbari, A. Nasajpour, Y. S. Zhang, A. Tamayol, A. Khademhosseini, *Adv. Drug Delivery Rev.* **2016**, *105*, 255; e) Y. Liu, J. Liu, S. Chen, T. Lei, Y. Kim, S. Niu, H. Wang, X. Wang, A. M. Foudeh, J. B. H. Tok, Z. Bao, *Nat. Biomed. Eng.* **2019**, *3*, 58; f) I. Bita, J. K. W. Yang, Y. S. Jung, C. A. Ross, E. L. Thomas, K. K. Berggren, *Science* **2008**, *321*, 939.
110. a) J. Sun, C. Zhang, Z. Yuan, X. Ji, Y. Fu, H. Li, M. Qin, *J. Phys. Chem. C* **2017**, *121*, 8976; b) M. Liao, P. Wan, J. Wen, M. Gong, X. Wu, Y. Wang, R. Shi, L. Zhang, *Adv. Funct. Mater.* **2017**, *27*, 1703852; c) G. Cai, J. Wang, K. Qian, J. Chen, S. Li, P. S. Lee, *Adv. Sci.* **2016**, *4*, 1600190.
111. a) G. H. Lee, S. H. Han, J. B. Kim, J. H. Kim, J. M. Lee, S.-H. Kim, *Chem. Mater.* **2019**, *31*, 8154; b) C. G. Schäfer, M. Gallei, J. T. Zahn, J. Engelhardt, G. P. Hellmann, M. Rehahn, *Chem. Mater.* **2013**, *25*, 2309; c) H. Chou, A. Nguyen, A. Chortos, J. W. F. To, C. Lu, J. Mei, T. Kurosawa, W. G. Bae, J. B. H. Tok, Z. Bao, *Nat. Commun.* **2015**, *6*, 8011; d) Y. Huang, J. Zhou, B. Su, L. Shi, J. Wang, S. Chen, L. Wang, J. Zi, Y. Song, L. Jiang, *J. Am. Chem. Soc.* **2012**, *134*, 17053; e) K. R. Phillips, G. T. England, S. Sunny, E. Shirman, T. Shirman, N. Vogel, J. Aizenberg, *Chem. Soc. Rev.* **2016**, *45*, 281; f) Z. Mao, H. Xu, D. Wang, *Adv. Funct. Mater.* **2010**, *20*, 1053; g) L. Wu, Z. Dong, M. Kuang, Y. Li, F. Li, L. Jiang, Y. Song, *Adv. Funct. Mater.* **2015**, *25*, 2237; h) L. Wang, J. Wang, Y. Huang, M. Liu, M. Kuang, Y. Li, L. Jiang, Y. Song, *J. Mater. Chem.* **2012**, *22*, 21405; i) H. Yi, S. H. Lee, H. Ko, D. Lee, W. G. Bae, T. i. Kim, D. S. Hwang, H. E. Jeong, *Adv. Funct. Mater.* **2019**, *29*, 1902720.
112. a) J. Ge, Y. Yin, *Angew. Chem. Int. Ed.* **2011**, *50*, 1492; b) Y. S. Zhang, A. Khademhosseini, *Science* **2017**, *356*, eaaf3627; c) K. Ellmer, *Nat. Photonics* **2012**, *6*, 809; d) F. Fu, Z. Chen, Z. Zhao, H. Wang, L. Shang, Z. Gu, Y. Zhao, *Proc. Natl. Acad. Sci. U. S. A.* **2017**, *114*, 5900; e) H. Kang, J. S. Lee, W. S. Chang, S. H. Kim, *Adv. Mater.* **2014**, *27*, 1282; f) Y. Heo, H. Kang, J. S. Lee, Y. K. Oh, S. H. Kim, *Small* **2016**, *12*, 3819; g) Z. Zhang, Z. Chen, L. Sun, X. Zhang, Y. Zhao, *Nano Res.* **2019**, *12*, 1579; h) Z. Zhang, Z. Chen, Y. Wang, J.

Chi, Y. Wang, Y. Zhao, *Small Methods* **2019**, *3*, 1900519; i) C. Shao, Y. Liu, J. Chi, J. Wang, Z. Zhao, Y. Zhao, *Research* **2019**, *2019*, 9783793.
113. Z. Zhang, Z. Chen, Y. Wang, Y. Zhao, *Proc. Natl. Acad. Sci. U. S. A.* **2020**, *117*, 18310.
114. a) J. Zheng, P. Xiao, X. Le, W. Lu, P. Théato, C. Ma, B. Du, J. Zhang, Y. Huang, T. Chen, *J. Mater. Chem. C* **2018**, *6*, 1320; b) J. Dong, J. Ding, J. Weng, L. Dai, *Macromol. Rapid Commun.* **2013**, *34*, 659; c) T. X. Li, N. Kong, S. S. Gao, P. Sui, Y. H. Zhao, C. Q. Yuan, *Adv. Mat. Res.* **2011**, *250–253*, 695.
115. D. Qu, H. Zheng, H. Jiang, Y. Xu, Z. Tang, *Adv. Opt. Mater.* **2019**, *7*, 1801395.
116. M. Xu, Z. Xu, M. A. Soto, Y. T. Xu, W. Y. Hamad, M. J. MacLachlan, *Adv. Mater.* **2023**, *35*, 2301060.
117. a) Q. Liu, M. G. Campbell, J. S. Evans, I. I. Smalyukh, *Adv. Mater.* **2014**, *26*, 7178; b) A. Querejeta-Fernández, G. Chauve, M. Methot, J. Bouchard, E. Kumacheva, *J. Am. Chem. Soc.* **2014**, *136*, 4788; c) A. Lukach, H. Thérien-Aubin, A. Querejeta-Fernández, N. Pitch, G. Chauve, M. Méthot, J. Bouchard, E. Kumacheva, *Langmuir* **2015**, *31*, 5033.
118. P. X. Wang, W. Y. Hamad, M. J. MacLachlan, *Nat. Commun.* **2016**, *7*, 11515.
119. J. A. Diaz, X. Wu, A. Martini, J. P. Youngblood, R. J. Moon, *Biomacromolecules* **2013**, *14*, 2900.
120. M. Ličen, B. Majaron, J. Noh, C. Schütz, L. Bergström, J. Lagerwall, I. Drevenšek-Olenik, *Cellulose* **2016**, *23*, 3601.
121. a) B. J. Lemaire, P. Davidson, D. Petermann, P. Panine, I. Dozov, D. Stoenescu, J. P. Jolivet, *Eur. Phys. J. E* **2004**, *13*, 309; b) J. Fresnais, J. F. Berret, B. Frka-Petesic, O. Sandre, R. Perzynski, *Adv. Mater.* **2008**, *20*, 3877; c) M. E. Leunissen, H. R. Vutukuri, A. van Blaaderen, *Adv. Mater.* **2009**, *21*, 3116; d) P. Dommersnes, Z. Rozynek, A. Mikkelsen, R. Castberg, K. Kjerstad, K. Hersvik, J. Otto Fossum, *Nat. Commun.* **2013**, *4*, 2066; e) B. Bharti, O. D. Velev, *Langmuir* **2015**, *31*, 7897; f) K. May, A. Eremin, R. Stannarius, S. D. Peroukidis, S. H. L. Klapp, S. Klein, *Langmuir* **2016**, *32*, 5085.
122. D. Jiao, F. Lossada, J. Guo, O. Skarsetz, D. Hoenders, J. Liu, A. Walther, *Nat. Commun.* **2021**, *12*, 1312.
123. a) S. Chen, G. Jiang, J. Zhou, G. Wang, Y. Zhu, W. Cheng, G. Xu, D. Zhao, H. Yu, *Adv. Funct. Mater.* **2023**, *33*, 2214382; b) B. Zhao, H. Wu, Q. Tian, Y. Li, F. Qiu, T. Zhang, *ACS Appl. Mater. Interfaces* **2023**, *15*, 8751.
124. L. D. C. de Castro, T. A. P. Engels, O. N. Oliveira, A. P. H. J. Schenning, *ACS Appl. Mater. Interfaces* **2024**, *16*, 14144.
125. X. X. Wen, Y. F. Yue, C. X. Wang, J. X. Zhang, Y. C. Xie, Y. Y. Ning, J. N. Li, X. G. Lu, S. Yang, *Adv. Funct. Mater.* **2024**, *34*, 2408792.
126. A. Barhoumi Meddeb, I. Chae, A. Han, S. H. Kim, *Cellulose* **2020**, *27*, 7901.
127. M. Kim, J. Jeon, K. Pierce, D. Bukharina, W. Choi, J. Choi, D. Nepal, M. E. McConney, T. J. Bunning, V. V. Tsukruk, *ACS Nano* **2024**, *18*, 25512.
128. P. Li, L. Li, K. J. Jeong, X. Yu, X. Yu, Y. Xu, *Adv. Opt. Mater.* **2022**, *10*, 2102616.
129. B. Frka-Petesic, G. Guidetti, G. Kamita, S. Vignolini, *Adv. Mater.* **2017**, *29*, 1701469.
130. a) M. Su, Z. Huang, Y. Li, X. Qian, Z. Li, X. Hu, Q. Pan, F. Li, L. Li, Y. Song, *Adv. Mater.* **2018**, *30*, 1703963; b) D. Gur, B. A. Palmer, S. Weiner, L. Addadi, *Adv. Funct. Mater.* **2016**, *27*, 1603514; c) Y. Meng, F. Liu, M. M. Umair, B. Ju, S. Zhang, B. Tang, *Adv. Opt. Mater.* **2018**, *6*, 1701351; d) F. Song, Z. Zhao, Z. Liu, J. W. Y. Lam, B. Z. Tang, *J. Mater. Chem. C* **2020**, *8*, 3284; e) F. Song, Y. Cheng, Q. Liu, Z. Qiu, J. W. Y. Lam, L. Lin, F. Yang, B. Z. Tang, *Mater. Chem. Front.* **2019**, *3*, 1768; f) J. Li, C. Hou, C. Huang, S. Xu, X. Peng, Q. Qi, W. Y. Lai, W. Huang, *Research* **2020**, *2020*, 3839160; g) J. Li, X. Peng, C. Huang, Q. Qi, W. Y. Lai, W. Huang, *Polym. Chem.* **2018**, *9*, 5278; h) J. Li, C. Yang, X. Peng, Q. Qi, Y. Li, W. Y. Lai, W. Huang, *Org. Biomol. Chem.* **2017**, *15*, 8463.
131. a) Z. Zhao, H. Wang, L. Shang, Y. Yu, F. Fu, Y. Zhao, Z. Gu, *Adv. Mater.* **2017**, *29*, 1704569; b) E. Yablonovitch, *Phys. Rev. Lett.* **1987**, *58*, 2059; c) W. Hong, Z. Yuan, X. Chen, *Small* **2020**, *16*, e1907626.
132. J. Gao, Y. Tang, D. Martella, J. Guo, D. S. Wiersma, Q. Li, *Responsive Mater.* **2023**, *1*, e20230008.
133. a) X. Wang, K. Yang, B. Zhao, J. Deng, *Small* **2024**, *20*, e2404576; b) J. Liu, Z. P. Song, J. Wei, J. J. Wu, M. Z. Wang, J. G. Li, Y. Ma, B. X. Li, Y. Q. Lu, Q. Zhao, *Adv. Mater.* **2024**, *36*, e2306834; c) J. Liu, J. J. Wu, J. Wei, Z. J. Huang, X. Y. Zhou, J. Y. Bao, R. C. Lan, Y. Ma, B. X. Li, H. Yang, Y. Q. Lu, Q. Zhao, *Angew. Chem. Int. Ed.* **2024**, *63*, e202319536; d) J. Liu, Z. P. Song, L. Y. Sun, B. X. Li, Y. Q. Lu, Q. Li, *Responsive Mater.* **2023**, *1*, e20230005; e) W. Kang, Y. Tang, X. Meng, S. Lin, X. Zhang, J. Guo, Q. Li, *Angew. Chem. Int. Ed.* **2023**, *62*, e202311486.
134. a) X. Zhang, Y. Xu, C. Valenzuela, X. Zhang, L. Wang, W. Feng, Q. Li, *Light Sci. Appl.* **2022**, *11*, 223; b) S. Lin, Y. Tang, W. Kang, H. K. Bisoyi, J. Guo, Q. Li, *Nat. Commun.* **2023**, *14*, 3005.
135. Z. Zheng, H. Hu, Z. Zhang, B. Liu, M. Li, D.-H. Qu, H. Tian, W.-H. Zhu, B. L. Feringa, *Nat. Photonics* **2022**, *16*, 226.
136. Y. Sang, J. Han, T. Zhao, P. Duan, M. Liu, *Adv. Mater.* **2020**, *32*, 1900110.
137. G. Chu, X. Wang, T. Chen, W. Xu, Y. Wang, H. Song, Y. Xu, *J. Mater. Chem. C* **2015**, *3*, 3384.
138. a) H. Zheng, W. Li, W. Li, X. Wang, Z. Tang, S. X. A. Zhang, Y. Xu, *Adv. Mater.* **2018**, *30*, 1705948; b) J. He, K. Bian, N. Li, G. Piao, *J. Mater. Chem. C* **2019**, *7*, 9278; c) H. Yu, B. Zhao, J. Guo, K. Pan, J. Deng, *J. Mater. Chem. C* **2020**, *8*, 1459.
139. a) H. Zheng, B. Ju, X. Wang, W. Wang, M. Li, Z. Tang, S. X.-A. Zhang, Y. Xu, *Adv. Opt. Mater.* **2018**, *6*, 1801246; b) E. Lizundia, T. D. Nguyen, J. L. Vilas, W. Y. Hamad, M. J. MacLachlan, *Mater. Chem. Front.* **2017**, *1*, 979.
140. Y. Shi, Z. Zhou, X. Miao, Y. J. Liu, Q. Fan, K. Wang, D. Luo, X. W. Sun, *J. Mater. Chem. C* **2020**, *8*, 1048.
141. a) F. Zhang, Q. Li, C. Wang, D. Wang, M. Song, Z. Li, X. Xue, G. Zhang, G. Qing, *Adv. Funct. Mater.* **2022**, *32*, 2204487; b) M. Kim, H. Lee, R. T. Snipes, M. J. Han, V. V. Tsukruk, *Small* **2021**, *18*, 2104340.
142. D. Lu, M. Li, X. Gao, X. Yu, L. Wei, S. Zhu, Y. Xu, *ACS Nano* **2022**, *17*, 461.
143. C. Duan, B. Wang, J. Li, J. Xu, J. Zeng, J. Li, Z. Zhao, W. Gao, G. Ying, K. Chen, *Small* **2022**, *18*, 2204199.
144. J. Tao, C. Zou, H. Jiang, M. Li, D. Lu, S. Mann, Y. Xu, *CCS Chem.* **2021**, *3*, 932.
145. X. Wu, W. Li, P. Wu, C. Ma, Y. Liu, M. Xu, S. Liu, *Eng. Sci.* **2018**, *4*, 111.
146. W. Li, M. Xu, C. Ma, Y. Liu, J. Zhou, Z. Chen, Y. Wang, H. Yu, J. Li, S. Liu, *ACS Appl. Mater. Interfaces* **2019**, *11*, 23512.
147. Y. Huang, Y. Qian, Y. Chang, J. Yu, Q. Li, M. Tang, X. Yang, Z. Liu, H. Li, Z. Zhu, W. Li, F. Zhang, G. Qing, *Adv. Mater.* **2024**, *36*, 2308742.
148. W. Sun, B. Tian, B. An, R. Teng, M. Xu, C. Ma, Z. Chen, H. Yu, J. Li, W. Li, S. Huan, S. Liu, O. J. Rojas, *Aggregate* **2024**, *6*, e712.
149. a) Y. Gong, L. Zhao, Q. Peng, D. Fan, W. Z. Yuan, Y. Zhang, B. Z. Tang, *Chem. Sci.* **2015**, *6*, 4438; b) W. Huang, C. Fu, Z. Liang, K. Zhou, Z. He, *Angew. Chem. Int. Ed.* **2022**, *61*, e202202977; c) H. R. Fu, N. Wang, X. X. Wu, F. F. Li, Y. Zhao, L. F. Ma, M. Du, *Adv. Opt. Mater.* **2020**, *8*, 2000330; d) Z. Huang, Z. He, B. Ding, H. Tian, X. Ma, *Nat. Commun.* **2022**, *13*, 7841.
150. a) S. An, L. Gao, A. Hao, P. Xing, *ACS Nano* **2021**, *15*, 20192; b) J. Liu, H. Zhang, N. Wang, Y. Yu, Y. Cui, J. Li, J. Yu, *ACS Mater. Lett.* **2019**, *1*, 58; c) L. Gu, W. Ye, X. Liang, A. Lv, H. Ma, M. Singh, W. Jia, Z. Shen, Y. Guo, Y. Gao, H. Chen, D. Wang, Y. Wu, J. Liu, H. Wang, Y. X. Zheng, Z. An, W. Huang, Y. Zhao, *J. Am. Chem. Soc.* **2021**, *143*, 18527; d) R. Liu, B. Ding, D. Liu, X. Ma, *Chem. Eng. J.*

2021, *421*, 129732; e) Z. Li, Y. Han, F. Nie, M. Liu, H. Zhong, F. Wang, *Angew. Chem. Int. Ed.* **2021**, *60*, 8212; f) Y. Jiang, C. Zhang, R. Wang, Y. Lei, W. Dai, M. Liu, H. Wu, Y. Tao, X. Huang, *Adv. Opt. Mater.* **2023**, *12*, 2302482.

151. a) J. Wei, C. Liu, J. Duan, A. Shao, J. Li, J. Li, W. Gu, Z. Li, S. Liu, Y. Ma, W. Huang, Q. Zhao, *Nat. Commun.* **2023**, *14*, 627; b) J. Wei, M. Zhu, T. Du, J. Li, P. Dai, C. Liu, J. Duan, S. Liu, X. Zhou, S. Zhang, L. Guo, H. Wang, Y. Ma, W. Huang, Q. Zhao, *Nat. Commun.* **2023**, *14*, 4839.
152. M. Cao, Y. Ren, Y. Wu, J. Shen, S. Li, Z.-Q. Yu, S. Liu, J. Li, O. J. Rojas, Z. Chen, *Nat. Commun.* **2024**, *15*, 2375.
153. X. Wang, Q. Miao, W. Zhang, Y. Zhou, R. Xiong, Y. Duan, X. Meng, C. Ye, *Chem. Eng. J.* **2024**, *481*, 148463.
154. K. Jin, C. Yin, J. You, H. Diao, J. Wang, K. Zhu, J. Zhang, J. Zhang, *Innov. Mater.* **2024**, *2*, 100096.
155. M. M. Liu, X. J. Wang, X. S. Pan, M. C. Geng, Y. Liu, Z. J. Zhang, H. B. Liu, M. Gao, *Carbohydr. Polym.* **2025**, *347*, 122767.
156. a) L. Bai, H. Wu, J. Ding, A. Ding, X. Zhang, N. Ren, G. Li, H. Liang, *Chem. Eng. J.* **2020**, *382*, 122919; b) M. Jonoobi, A. Ashori, V. Siracusa, *Polym. Test.* **2019**, *76*, 333; c) C. Balcik-Canbolat, B. Van der Bruggen, *Cellulose* **2020**, *27*, 5255; d) D. Zhang, A. Karkooti, L. Liu, M. Sadrzadeh, T. Thundat, Y. Liu, R. Narain, *J. Membr. Sci.* **2018**, *549*, 350; e) P. Daraei, N. Ghaemi, H. Sadeghi Ghari, M. Norouzi, *Cellulose* **2016**, *23*, 2025; f) F. Lessan, M. Karimi, J. L. Bañuelos, R. Foudazi, *Polymer* **2020**, *186*, 121969; g) S. Zheng, S. Yang, Z. Ouyang, Y. Zhang, *Appl. Surf. Sci.* **2023**, *614*, 156157; h) A. Aguilar-Sanchez, B. Jalvo, A. Mautner, S. Nameer, T. Pöhler, T. Tammelin, A. P. Mathew, *J. Membr. Sci.* **2021**, *620*, 118842.
157. H. Xie, Y. Xu, D. Lu, A. Wang, Y. Niu, J. Wei, X. Wang, C. Si, *Sep. Purif. Technol.* **2025**, *355*, 129815.
158. a) Y. Liu, F. Han, F. Li, Y. Zhao, M. Chen, Z. Xu, X. Zheng, H. Hu, J. Yao, T. Guo, W. Lin, Y. Zheng, B. You, P. Liu, Y. Li, L. Qian, *Nat. Commun.* **2019**, *10*, 2409; b) K. Jiang, S. Sun, L. Zhang, Y. Lu, A. Wu, C. Cai, H. Lin, *Angew. Chem. Int. Ed.* **2015**, *54*, 5360.
159. a) P. She, Y. Ma, Y. Qin, M. Xie, F. Li, S. Liu, W. Huang, Q. Zhao, *Matter* **2019**, *1*, 1644; b) Z. Zeng, B. Huang, X. Wang, L. Lu, Q. Lu, M. Sun, T. Wu, T. Ma, J. Xu, Y. Xu, S. Wang, Y. Du, C. H. Yan, *Adv. Mater.* **2020**, *32*, 2004506; c) X. Yu, L. Wu, D. Yang, M. Cao, X. Fan, H. Lin, Q. Zhong, Y. Xu, Q. Zhang, *Angew. Chem. Int. Ed.* **2020**, *59*, 14527.
160. a) L. Gu, H. Wu, H. Ma, W. Ye, W. Jia, H. Wang, H. Chen, N. Zhang, D. Wang, C. Qian, Z. An, W. Huang, Y. Zhao, *Nat. Commun.* **2020**, *11*, 944; b) J. Tan, Q. Li, S. Meng, Y. Li, J. Yang, Y. Ye, Z. Tang, S. Qu, X. Ren, *Adv. Mater.* **2021**, *33*, 2006781.
161. a) X. Li, Y. Xie, B. Song, H. L. Zhang, H. Chen, H. Cai, W. Liu, Y. Tang, *Angew. Chem. Int. Ed.* **2017**, *56*, 2689; b) J. Andres, R. D. Hersch, J. E. Moser, A. S. Chauvin, *Adv. Funct. Mater.* **2014**, *24*, 5029.
162. Q. Qin, Y. Xu, *Adv. Sci.* **2024**, *11*, 2404761.
163. K. Fleming, D. G. Gray, S. Matthews, *Chemistry* **2001**, *7*, 1831.

AUTHOR BIOGRAPHIES

Dr. Jiao Liu received her Ph.D. degree in Advanced Material and Liquid Crystal Institute (AMLCI) at Kent State University in 2022. She is currently an assistant professor at Nanjing University of Posts and Telecommunications. Her research focuses on circularly polarized luminescent liquid crystal materials, chiral liquid crystal elastomer, lyotropic liquid crystals, and the stimuli-responsive soft matter.

Dr. Ye-Ming Qing is an Associate Professor & Special-Term Professor of Nanjing University of Posts and Telecommunications. He received the Ph.D. degree in Electromagnetic and Microwave Technology from Southeast University, Nanjing, China, in 2022. His research interests mainly focus on manipulating the light flow and light-matter using optically resonant nanostructures, engineering the complex nanophotonic response through structured nanoscale materials, and developing the theory and modeling tools for novel nanophotonic, plasmonic, optoelectronic devices.

Dr. Jun-Jie Wu is currently a graduate student in Nanjing University of Posts and Telecommunications. His research mainly focuses on cholesteric liquid crystal, circularly polarized luminescent materials and liquid crystal elastomer.

Jing-Qi Tian is currently a graduate student at Nanjing University of Posts and Telecommunications. His research mainly focuses on cholesteric liquid crystal and liquid crystal planar photonics.

Chi-Bo Feng is currently a graduate student at Nanjing University of Posts and Telecommunications. His research mainly focuses on circularly polarized luminescent liquid crystal materials, circularly polarized organic ultralong room-temperature phosphorescence materials, and stimuli-responsive soft matter.

Xin-Yu Zhou is currently a graduate student in Nanjing University of Posts and Telecommunications. His research mainly focuses on circularly polarized luminescent liquid crystal materials, chiral liquid crystal elastomers, and stimuli-responsive soft matter.

Yun Ma obtained his PhD degree from Hong Kong Baptist University in 2015. He is currently a full professor at State Key Laboratory of Flexible Electronics (LoFE), Nanjing University of Post & Telecommunications. His research interests include stimuli-responsive organic materials, organic scintillators for x-ray detection, organic circularly polarized luminescent materials and devices.

Bing-Xiang Li received his Ph.D. degree in Chemical Physics from Advanced Material and Liquid Crystal Institute at Kent State University in 2019. He is currently a professor in Nanjing University of Posts and Telecommunications. His current research spans from liquid crystals, stimuli-responsive soft matter, active matter, to biological physics.

Yan-Qing Lu received both his B.S. and Ph.D. degrees from Nanjing University, China, in 1991 and 1996, respectively. He has 5 years of experience in telecom industries in the United States and China. He is currently a Changjiang Distinguished Professor at Nanjing University and a Fellow of the Optical Society of America and Chinese Optical Society. His research interests include liquid crystal photonics, fiber optics, and nonlinear optics.

Quan Li is Distinguished Chair Professor and Director of Institute of Advanced Materials at Southeast University. He held appointments in USA, Germany, and France. Li received his Ph.D. from Chinese Academy of Sciences in Shanghai, where he was promoted to a youngest Full Professor in February 1998. He is a Fellow of the Royal Society of Chemistry. He has been elected as a member of the European Academy of Sciences and the European Academy of Sciences and Arts. He has also been honored as Professor and Chair Professor at ten universities. His current research interest spans from stimuli-responsive smart soft matter, advanced photonics, and optoelectronic materials for energy harvesting and energy saving to functional biocompatible materials, biomedical materials, and nanoparticles to nanoengineering and device fabrication.

How to cite this article: J. Liu, Y.-M. Qing, J.-J. Wu, J.-Q. Tian, C.-B. Feng, X.-Y. Zhou, Y. Ma, B.-X. Li, Y.-Q. Lu, Q. Li, *Responsive Mater*. **2025**, e70020. https://doi.org/10.1002/rpm2.70020